BEHAVIOR OF REINFORCED CONCRETE MASONRY WALLS SUBJECTED TO COMBINED AXIAL LOADING AND OUT-OF-PLANE BENDING

by

Kun Hu

Submitted
in partial fulfillment of the requirements
for the degree of

MASTER OF APPLIED SCIENCE

at

DALHOUSIE UNIVERSITY

Halifax, Nova Scotia September, 2005

DALHOUSIE UNIVERSITY

To comply with the Canadian Privacy Act the National Library of Canada has requested that the following pages be removed from this copy of the thesis:

Preliminary Pages
- Examiners Signature Page
- Dalhousie Library Copyright Agreement

Appendices
- Copyright Releases (if applicable)

TABLE OF CONTENTS

PAGE

LIST OF TABLES

PAGE

LIST OF FIGURES

PAGE

LIST OF ABBREVIATIONS AND SYMBOLS USED

A	total net area of a cross-section
ACI	American Concrete Institute
ASCE	American Society of Civil Engineers
ASTM	American Society for Testing and Materials
ASWG	American Steel Wire Gage
b	width of cross-section
C_m	coefficient for equivalent uniform bending
C.O.V	Coefficient of Variation
CSA	Canadian Standards Association
e	load eccentricity
e_1	the smaller eccentricity applied at top or bottom of member
e_2	the larger eccentricity applied at top or bottom of member
e_a	eccentricity of axial load, which generates out-of-plane bending
e_f	flexural eccentricity due to lateral load
e_k	kern eccentricity
E	Young's modulus
E_i	initial, tangent modulus of elasticity
E_m	modulus of elasticity of masonry
y_0	the distance of vertical force from the compression face at wall mid-height
f_y	yield strength of steel reinforcement
f'_m	compressive strength of masonry
h	height of a wall or column
H	lateral load
HSS	Hollow Structural Section

I	net section moment of inertia
I_0	same as I
I_{cr}	moment of inertia of cracked section
I_{eff}	effective moment of inertia
I_{end1}	net section moment of inertia at one end taking eccentricity into consideration
I_{end2}	net section moment of inertia at one end taking eccentricity into consideration
I_n	initial moment of inertia, same as I
k	effective height factor for compression member
kN	kiloNewton
LEED	Leadership in Energy and Environmental Design
LVDT	Linear Variable Differential Transducer
mm	millimeter
M	bending moment
M_1	the lesser bending moment
M_2	the larger bending moment
M_f	factored moment
M_p	primary moment
M_s	secondary moment
M_{theory}	theoretically predicted moment capacity
M_u	maximum bending moment capacity
MPa	Mega Pascal
n	degree of nonlinearity of masonry stress-strain curve
P	axial load in wall or column
P_0	masonry wall axial capacity determined from prism tests
P_f	factored applied axial load

P_{cr}	critical buckling load
P_{max}	maximum axial load
P_{theory}	theoretically predicted axial load capacity
P_u	ultimate axial load capacity
r	radius of gyration
R	reduction factor
R^2	correlation coefficient
t	effective thickness of wall or column
TMS	The Masonry Society
β_d	creep effect factor (factored dead load moment/factored total moment)
δ_m	deflection at ultimate
Δ	lateral deflection
Δ_u	deflection at ultimate, same as δ_m
ε	strain
ε_1	maximum strains on the compression surfaces
ε_2	minimum strains on the tension surfaces
λ	moment diagram coefficient

ACKNOWLEDGEMENTS

I would like to take this opportunity to publicly express my gratitude to all those people who have helped me in the course of my research and writing up this thesis.

First and foremost, I gladly acknowledge my debt to my supervisor Dr. Yi Liu. I could not have imagined having a better advisor and mentor for my M.A.Sc and without her constant friendship, understanding, encouragement and advice over the last two years I would never have finished. Thank-you to my committee members, Dr. Jane Thorburn (internal) and Dr. John Dawe (external) from University of New Brunswick, for providing guidance and evaluation throughout this project and managing to read the whole thesis so thoroughly. The financial support from NSERC is greatly appreciated.

Mark MacDonald, Blair Nickerson and Brian Liekens contributed their technical experience and assistance throughout the experimental part of this research. I especially thank my many student colleagues at the Department of Civil Engineering at Dalhousie University, and particularly James Hou, Meg Tang, Simon Yang, Jeffery Qu, Haipeng Han, and Dr. Jinquan Chen. All of them made my study here a cherished memory.

Lastly, and most importantly, I wish to thank my parents Baosheng Hu and Yuanbao Wen and my sister Wei Hu for their non-stopped material and moral support. To them I dedicate this thesis.

ABSTRACT

An experimental program was designed and conducted to study the strength and behavior of masonry load-bearing walls. Ten reinforced large-scale wall specimens with pinned support conditions were tested under eccentric compressive loading. The load eccentricities at two ends of the specimen were applied in a manner which resulted in various specimen bending patterns. Four of these specimens were tested under symmetrical single curvature loading, three of them were tested under asymmetrical single curvature bending, and the remaining three were tested under reverse curvature bending. Wall specimens were 2390 mm high by 790 mm long by 140 mm thick, which resulted in a slenderness ratio of 17.1. Ultimate load and corresponding applied moment, and lateral deflections at critical cross-sections were obtained and presented in either table or graph format. Moment vs. curvature curves were established and used to determine effective flexural rigidities, EI_{eff}, at the time of failure of walls under various loading conditions. Results of large-scale tests showed that for a constant end eccentricity ratio, e_1/e_2, the ultimate load and the associated EI_{eff} decreased as the end eccentricity ratio, e/t, increased. The ultimate load and the EI_{eff} values increase as the end eccentricity ratio, e_1/e_2, varied from 1.0 to 0.0 and to -1.0. This increase in the strength and flexural rigidity was attributed to a change of the failure mode from tension-controlled failure to compression-controlled failure associated with the change of e_1/e_2. A comparison study revealed that similar effects of e/t and e_1/e_2 on the capacity and EI_{eff} of the walls was noted in other relevant research. Through the comparison, an increase of EI_{eff} with the increased slenderness ratio, h/t, was also believed to occur. While test results obtained by others supported the findings in this research with regard to the effects of e/t and e_1/e_2 on the capacity of the wall, the effect of h/t on the EI_{eff} values remained inconclusive due to limited test data.

The measured ultimate loads and flexural rigidities were also compared with the predicted code values. The results showed that the current Canadian masonry design code, S304.1-M04, tends to underestimate the capacity and effective flexural rigidity of masonry walls and thus leads to a conservative design over a range of parameters. This underestimation is most significant in compression-controlled failure regions. In the regions of tension-controlled failure, the code appears to agree reasonably well with the available data. Several existing equations for determining EI_{eff} were also evaluated with regard to their accuracy and validity for application based on the available tested data.

CHAPTER I INTRODUCTION

1.1. Background of Masonry Development

The use of masonry dates back as early as ten thousand years ago in ancient Turkey. Since then, masonry has been one of the principal construction materials till late nineteenth century. Existing spectacular masonry structures across the world are unarguable testimonials of masonry's once glorious history. However, masonry construction experienced a serious decline in the past 100 years due to its slow development in construction techniques and more importantly, a rational design method. While rational design methods and building codes were rapidly developing for the other more modern construction materials such as concrete and steel, masonry was being designed by very conservative "rules of the thumb" based on its historical use. Such rules of thumb lead to inordinately high safety factors combined with unacceptably high construction costs in our modern engineering age. Not until the 1960s was masonry revived as a competitive construction material with the introduction of American Standards Association Building Code Requirement for Masonry (ASA A41.4-1953) and the National Building Code of Canada (1965) together with significant improvements in masonry manufacturing techniques.

From the 1960s to 1980s, most countries including Canada adopted working stress design for masonry structural elements in which the maximum stresses in elements were limited to allowable stresses as specified by the Canadian masonry code (CSA S304.1–84). Based on more reliable experimental and analytical research, CSA issued a design standard for masonry in 1994 (CSA S304.1-M94) using the limit states design philosophy to achieve a more consistent factor of safety and to better utilize the material load-carrying potential. Based on the limit states design, the most recent CSA structural design standard for masonry (CSA S304.1-M04) issued in 2004 reflected the important

research findings gathered in the past decade and appropriate changes were made to the 1994 edition to provide more uniform and economical design guidelines. By applying these design methods, the number of storeys in masonry buildings has increased substantially while bearing wall thicknesses have decreased. In recent years, with the introduction of LEED (Leadership in Energy and Environmental Design) Green Building Rating system (2000) for building construction and design and an increased public awareness for the environment, masonry, recognized as an energy efficient and environmental friendly materials, has regained its competitiveness in the construction market. As a result, the research attention in more efficient use and design of masonry material has increased to keep pace with the growing development of masonry construction.

1.2 Secondary Effect (Slenderness Effect)

Masonry was traditionally used as a structural element to resist compression in the form of load-bearing walls and columns. A considerable amount of previous research has been dedicated to the study of masonry behavior under pure axial compression. However, a larger portion of masonry elements are required to resist combined axial load and out-of-plane bending due to wind, earthquake or eccentric compressive load. It has been shown that the resistance of structural elements to a combination of axial load and bending is governed by the interaction of material response and structural stability. For short walls and columns, material failure characterized by either steel yielding or masonry crushing dominates. Very slender walls and columns exhibit stability failure in which members collapse while stresses caused by external loads are still within the acceptable limits of the material. Walls and columns with dimensions and support conditions that result in intermediate slenderness commonly occur in practice. When tested in the laboratory, such specimens exhibit failure modes that manifest the

interaction of material failure and member stability characteristics. The member strength is compromised by a secondary moment effect also referred to as the slenderness effect. This effect may be evaluated using an iterative process that the lateral deflection due to a primary moment results in additional moment with subsequent additional deflection. Due to the low tensile strength of masonry, this situation is further complicated by tension cracking which occurs first where the moment is maximum. The deepening of tension cracks reduces the effective moment of inertia at a section and the reduced effective compression area in turn, results in increased stress. The higher stress leads to a reduction in the value of Young's modulus, E_m, for masonry which results from a typically non-linear masonry stress-strain constitutive relationship. In addition, variation of the development of tensile cracks along the member height leads to variations in effective section properties over the member height. Therefore, any rational design method for such masonry elements must consider simultaneous changes in the moment of the inertia, I, and Young's modulus, E_m. Typically, these values are embodied in a single term, $(EI)_{eff}$, referred to as "*EI* effective".

The current Canadian masonry design code (CSA S304.1-M04) suggests the use of either of two methods to account for this secondary effect: an iterative load-displacement procedure and a single step moment magnifier procedure. In both cases, the member is designed for a magnified moment calculated on the basis of a semi-empirical expression for EI_{eff} which is proposed to account for the reduced flexural rigidity of masonry elements at failure.

1.3 Objectives

In light of the discussion above, the research presented herein was initiated to accomplish the following:

1. to provide an extensive review of available literature on research related to the behavior of masonry load-bearing walls;
2. to conduct an experimental program to evaluate behavior and capacity of masonry wall specimens subjected simultaneously to simulated gravity load and out-of-plane bending;
3. to design a test set-up capable of realizing loading conditions required for the experimental program;
4. to conduct an auxiliary test program to obtain material properties of masonry prism and masonry components including blocks, mortar, grout and reinforcement;
5. to conduct a parametric study investigating the effects of slenderness ratio and loading conditions on the behavior, capacity and EI_{eff} of masonry walls;
6. to examine the validity of the currently recommended design procedures including an assessment of the efficacy of the EI effective values;
7. to present appropriate conclusions and recommendations resulting from this research.

1.4 Scope of Research

This research includes a review of literature, laboratory testing of 10 large-scale reinforced concrete masonry walls under eccentric compressive load with varying eccentricities and end moment conditions. Auxiliary testing of masonry prisms and masonry components is conducted along with an in-depth evaluation of various existing equations for the determination of flexural rigidity values. The focus is primarily on the current code equations based on test data obtained in this research as well as from other literature.

A review of available literature related to the present work is included in Chapter II. Chapter III presents a detailed description of the experimental program including both large-scale wall tests and auxiliary tests. Results of auxiliary tests are also included in Chapter III. Results of large-scale wall tests are presented and analyzed in Chapter IV. Chapter V presents an analysis of the effects of several parameters on the capacity and EI_{eff} values and evaluates the validity of code equations using test data from this research and other available research. A summary and conclusions, as well as recommendations relevant to existing design guidelines are reported in Chapter VI.

CHAPTER II LITERATURE REVIEW

2.1. Introduction

Research on the strength of masonry load-bearing walls considering slenderness effect has been carried out both experimentally and analytically in past three decades on a wide variation of cross-sectional dimensions, materials, and slenderness ratios. The findings from the research have formed the basis of the current Canadian design guidelines (CSA S304.1-M04) for masonry wall design. However, while most reported research investigated the buckling capacity of walls under axial compressive loads with various combinations of eccentricities resulting in single curvature bending, little research has addressed the behavior, capacity and corresponding EI_{eff} for walls subjected to eccentric compressive loading which results in reverse curvature or asymmetrical single curvature bending. The most relevant research to this study is summarized in the following sections with the focus on studies of the critical buckling load, P_{cr}, and effective flexural rigidity, EI_{eff}.

2.2 Critical Buckling Load

Most of the past analyses of stability of masonry members have been developed by assuming that the member behaves elastically and that the masonry has little or no tensile strength. Chapman and Slatford (1957) considered the effect of the additional deflection resulting from the compressive loading acting through the deflected brick masonry wall. Based on assumptions of linear elastic behavior and zero tensile strength for masonry in tension, the authors obtained load-deflection relationship from governing differential equations for the deflected masonry wall. However, no specific expression for calculating critical buckling load was given to generate appropriate design equations.

Based on the solution of differential equations for deflection curve of a cracked plain masonry column with solid rectangular cross-section, Yokel and Dikkers (1971) and Hatzinikolas et al. (1978) each proposed an analytical solution, expressed in Equation (2.1), for determining the critical load of compression members with the assumption that the members are made of materials that exhibit no tensile strength and linear stress-strain relationship

$$P_{cr} = \frac{\pi^2 EI_0}{h^2}\left(1-\frac{2e}{t}\right)^3 \tag{2.1}$$

where E is the modulus of elasticity, I_0 is the moment of inertia of the uncracked masonry cross-section, h is the masonry member height and e and t are the eccentricity of the applied axial load and thickness of masonry cross-section, respectively.

Frisch-Fay (1975) extended the previous studies by considering both cracked and uncracked plain masonry members. He derived the load-deflection relationship for masonry columns by integrating the moment curvature relationships for the cracked and uncracked sections of a masonry column. Calibrated using the experimental data, Frisch-Fay arrived at the following equation for predicting the capacity of eccentrically loaded masonry piers:

$$P_{\max} = 7.7\frac{EI}{h^2}\left(\frac{1}{2}-\frac{e}{t}\right)^3 \tag{2.2}$$

where the symbols are defined as before.

In a research study conducted by Schultz and Mueffelman (2003) an elastic stability solution for slender unreinforced masonry walls subjected to transverse load and axial compression was presented. Based on the numerical approximation for the governing differential equation for bending of the unreinforced masonry walls, an equation to calculate the buckling capacity, P_{cr}, for a transversely loaded masonry member was

proposed, in which linear material property was assumed:

$$P_c = \frac{\pi^2 E_m I}{h_e^2}\left[1 - 0.577\left(\frac{e_a + \lambda e_f}{r}\right)\right]^3 \tag{2.3}$$

where e_a is the eccentricity of axial load while e_f is the flexural eccentricity defined as a ratio of bending moment caused by lateral loads to axial load. The value of λ is 1.0 for a simple span with constant moment, 0.905 for a simple span with a uniform lateral load, and 0.813 for a cantilever with a lateral point load at the free end. r is the radius of gyration and is given as:

$$r = \sqrt{\frac{I}{A}} = 0.289t \tag{2.4}$$

The authors demonstrated that the proposed elastic solution for buckling strength provides a conservative estimate of the buckling capacity of slender unreinforced masonry walls.

Based on the critical buckling load equations proposed by previous research, ACI 530/ASCE5/TMS 402-99 proposed the following equation to calculate the critical buckling load for a solid rectangular masonry cross-section:

$$P_e = \frac{\pi^2 EI}{h^2}\left(1 - 0.577\frac{e}{r}\right)^3 \tag{2.5}$$

where e is eccentricity of the applied vertical load, and all the other terms are as defined previously. It is required in the provision that the applied axial load must be less than 25 per cent of the critical load calculated by this equation.

Colville (1992) questioned the validity of Equation (2.5) based on a comprehensive theoretical study. He suggested that it may be unconservative for hollow or partially grouted masonry walls subjected to single curvature bending. A reduction factor was then proposed to modify Equation (2.5) and the modified equation is shown as follows:

$$P_e = \frac{\pi^2 E_m I}{h^2}\left(1 - 0.577\frac{e}{r}\right)^3 R \tag{2.6}$$

in which R is the reduction factor, a function of e/r which depends on the extent of cracking in a wall section and the grout spacing. Colville concluded that although this new equation is not exact, it is considered safe and practical for service load design use in concert with a factor of safety of 4.0.

Romano et al. (1993) studied the impact of nonlinearity in the masonry stress-strain relationship on the buckling capacity of brick masonry walls. They concluded that nonlinearity resulted in a large reduction of critical load capacities compared with the buckling strength of linear, elastic systems. For plain masonry walls subjected to a constant lateral load H, the maximum vertical load, P_{max}, that the wall can support can be obtained from the following expression with b h being the width and height of the wall, respectively:

$$P_{\max} = \frac{n+2}{n+1} b\left(y_0 - \frac{H}{P_{\max}} h\right) f'm \tag{2.7}$$

In this expression, n represents the degree of the material non-linearity, y_0 is the distance of the vertical force from the compression face at wall mid-height, and f'_m is the masonry compressive strength.

The equations summarized previously were based mainly on theoretical solutions of differential equations for unreinforced masonry walls under combined compression and bending including the effect of tensile cracking and, in some cases, the material nonlinearity of masonry. Certain empirical or semi-empirical factors were applied to these equations to obtain reasonably good correlation between the theoretical values and test data. However, in the case of partially grouted reinforced masonry walls, due to the addition of reinforcement, the differential equations are much more complicated than

those for plain walls, which makes it extremely difficult, if not impossible, to obtain the theoretical solutions. The theoretical solutions reported in the literature have adopted so many assumptions for simplification that the solution is no longer valid for a wide range of characteristics encountered in masonry walls in practice.

2.3 Flexural Rigidity

The following summarizes the experimental research conducted to determine the flexural rigidities of masonry members at failure including effects of tensile cracking and reinforcement.

Yokel and Dikkers (1971) developed an analytical solution for determining the capacity of slender masonry plain walls under various combinations of axial compression and transverse loading. The expression for calculating flexural rigidity, *EI*, at failure was proposed as following:

$$EI = E_i I_n (0.2 + \frac{P}{P_0}) \leq 0.7 E_i I_n \tag{2.8}$$

where E_i is the initial, tangent modulus of elasticity, P is the applied vertical load on the masonry at failure, I_n is the moment of inertia of the uncracked net cross-section, and $P_0 = f'_m bt$ is the axial capacity determined from prism tests with flat end conditions. This equation is the result of a study based on experimental data obtained for brick masonry walls tested under various combinations of axial compression and flexure. Yokel and Dikkers (1971) recommended that future research be done on the effects of section cracking and the change in E with increasing stress.

The accuracy of Equation (2.8) for short sections of brick walls, and possible application

to concrete masonry walls was investigated by Fattal and Cattaneo (1976) who tested eccentrically loaded short walls. They believed that in short walls the secondary moment produced by the axial load acting on transverse deflection, Δ, is negligible compared to the primary moment, Pe. Based on this consideration, they calculated the flexural rigidity, EI, from the following relationship:

$$EI = \frac{Pet}{\varepsilon_1 - \varepsilon_2} \tag{2.9}$$

where P is the axial load applied on the short wall, t is the wall thickness, e is the load eccentricity. ε_1 and ε_2 represent the maximum and minimum wall strains on the compression and tension surfaces, respectively. It was noted that for concrete block prisms, this equation gives underestimated wall capacity when compared with Equation (2.8).

Hatzinikolas et al. (1978) carried out an experimental program including tests on axially and eccentrically loaded plain and reinforced masonry walls. Based on the test results and combined with analytical investigation, they defined the moment of inertia of a cracked wall section, I_{cr}, as a function of the loading eccentricity:

$$I_{cr} = 8\left(\frac{1}{2} - \frac{e}{t}\right)^3 I_0 \tag{2.10}$$

in which t is the wall thickness, e is the eccentricity of the applied axial load, I_0 is the moment of inertia of the uncracked cross-section. The authors demonstrated that this equation is appropriate for evaluating the moment of inertia of plain masonry walls loaded in single curvature, and reinforced masonry walls subjected to single curvature bending with eccentricities less than one third of the wall thickness. Further research is recommended to provide more reliable information for more general cases considering reverse curvature bending and a non-linear stress-strain relationship for masonry.

For concrete masonry walls bent in single curvature with a single layer of reinforcement, MacGregor et al. (1974) recommended the use of the following equation for the flexural rigidity

$$E_m I = E_m I_0 \left(\frac{1}{2} - \frac{e}{t} \right) \geq 0.10 E_m I_0 \tag{2.11}$$

In this expression, E_m is the masonry modulus of elasticity, I is the moment of inertia of the masonry wall section. I_0 is the moment of inertia of the uncracked wall section, t is the wall thickness and e is the eccentricity of the applied load. Experimental results of eccentrically loaded concrete specimens showed that this expression gave reasonably good approximation of the flexural rigidity for masonry walls with a load eccentricity larger than $t/3$. The term, $0.10E_mI_0$, represents a minimum value of EI at failure afforded by the steel reinforcement, which would be zero for plain walls.

Finite element analysis was employed by Maksoud and Drysdale (1993) in a numerical investigation of slender unreinforced hollow concrete masonry walls. Both geometrical and material nonlinearities were included in the investigation to simulate the P-δ effect and the decrease of the wall stiffness due to the extension of cracks. The effective modulus of rigidity, EI_{eff}, described as a reduction factor R times the elastic modulus of rigidity, EI_0, was obtained as follows:

For single curvature walls (e_1/e_2=1.0, 0.0)

$$R = 0.1037 + 0.915\frac{e}{t} + 0.089\frac{e}{t}\frac{e_1}{e_2} + 0.00034\left(\frac{h}{t}\right)^2 - 0.0098\frac{e}{t}\frac{h}{t} \tag{2.12}$$

For reverse curvature walls (e_1/e_2=-1.0)

$$R = 0.3278 - 1.98\frac{e}{t}\frac{e_1}{e_2} + 0.0425\frac{e}{t}\frac{h}{t} + 0.00044\frac{h^2}{t} - 0.0146\frac{h}{t} \tag{2.13}$$

In these expressions, R increases with increasing e/t and with increasing h/t. The formulations represent an empirical approach based on the moment magnifier method

which, for masonry, requires additional verification. Consequently, the authors recommended that the influence of section geometries, material properties, reinforcement, and long term effects be incorporated in a comprehensive design approach.

Based on the experimental data for unreinforced brick and concrete block walls, Ojinaga and Turkstra (1980) demonstrated that the moment magnifier method can be very conservative for walls subjected to small eccentricities but becomes unconservative for those subjected to larger eccentricities. Based on the assumptions of linear stress-strain behavior and zero tensile strength of masonry, they proposed the following equations to determine the effective moment of inertia I_{eff} for plain brick or concrete block masonry wall sections:

$$I_{eff} = \frac{(I_{end1} + I_{end2})}{4} \qquad \text{for } 0 \le {e_1}/{e_2} \le \pm 1 \tag{2.14}$$

$$I_{eff} = \text{minimum}\begin{cases} (I_{end1} + I)/4 \\ (I_{end2} + I)/4 \end{cases} \qquad \text{for } -1 \le {e_1}/{e_2} \le 0 \tag{2.15}$$

where I_{end1} and I_{end2} are the moment of inertia at the wall end cross-sections considering only the primary moment caused by the eccentrically applied vertical load, and I is the net section moment of inertia.

In a follow-up research by Ojinaga and Turkstra (1981), Equations (2.14) and (2.15) were modified and a term, I_{cr}, defined as the moment of inertia of a cross-section under pure bending was introduced. The new equations are

for single curvature bending, $0 \le {e_1}/{e_2} \le 1$,

$$I_{eff} = \frac{(I_{end1} + 2I_{cr} + I_{end2})}{4} \tag{2.16}$$

and for reverse curvature bending, $-1 \le {e_1}/{e_2} \le 0$

$$I_{eff} = \text{minimum}\begin{cases}\dfrac{(I_{end1} + 2I_{cr} + I)}{4} \\ \dfrac{(I_{end2} + 2I_{cr} + I)}{4}\end{cases} \tag{2.17}$$

where I is the net section moment of inertia including the contribution, if any, of steel area transformed to equivalent masonry. Use of I_{cr} implies that, in the limit, the moment of inertia at the critical section just prior to failure is at least equal to the moment of inertia under pure moment. Compared with test results, the theory was found to be conservative especially for symmetrical single curvature cases.

In an experimental program conducted by Aridru (1997), seventy-two plain and reinforced concrete masonry walls with pinned-pinned support conditions were tested at various load eccentricities under axial compressive loading. Experimental results showed that for reinforced walls, EI_{eff} values determined experimentally were higher than those recommended by CSA S304-M94 for load eccentricity, e, ranging from $0.18t$ to $0.36t$. A proposed equation for EI_{eff} for reinforced masonry walls derived using curve fitting techniques on experimental data is expressed as:

$$(EI)_{eff} = 2.7E_m I_0 \exp\left(-7.5\frac{e}{t}\right) \quad \text{for } \frac{e}{t} \geq 0.18 \tag{2.18}$$

For load eccentricity ratio, e/t, less than 0.18, an empirical value of 0.7 was selected as the upper limit of the effective flexural rigidity of masonry walls. For load eccentricity ratio e/t, greater than or equal to 0.36, the values obtained from the proposed equation agree well with those recommended by CSA S304.1-M94.

A research program carried out by Liu (2002) included the testing of 36 reinforced concrete masonry walls and a numerical analysis of approximately 500 computer model tests. The program indicated that the effective flexural rigidity values at failure calculated according to the Canadian masonry code CSA-S304.1-M94 tend to underestimate EI

values for reinforced walls. Based on the numerical study of the behavior of concrete masonry load-bearing walls under various loading conditions, a lower bound tri-linear limit for the effective flexural rigidity of reinforced masonry walls was established as follows

$$\frac{EI_{eff}}{EI_0} = 1 - (2.375 - 0.0175\frac{h}{t})\left(\frac{e}{t}\right) \qquad (2.19)$$

for $0.1 \le e/t \le 0.4$

$$\frac{EI_{eff}}{EI_0} = \left(0.05 + 0.007\frac{h}{t}\right) \qquad (2.20)$$

for $e/t > 0.4$

where e is the value of the maximum end eccentricity for end-applied axial loads and maximum virtual eccentricity for combined axial loading and bending cases. For wall specimens with e/t less than 0.1, an upper limit of 0.8 was selected. These equations are believed to give accurate and realistic estimate of EI_{eff} when compared with test results.

2.4 Design Guidelines and Implications

For the design of plain and reinforced masonry load-bearing walls, the secondary effect is included using a load displacement method or a moment magnifier method in the current Canadian masonry design code (CSA S304.1-M04).

The load displacement method requires the determination of the maximum lateral deflection, δ_m, occurring at some point along the length of a member and caused by the primary moment, M_p. The primary moment causing deflection perpendicular to the plane of a wall may be due to eccentric axial loading, lateral loading, or both. A secondary moment, $P_f \delta_m$, results from compressive force, P_f, and is added to the primary moment

to give a total factored maximum moment. Since the secondary moment increases the deflection, further iterative calculations resulting in a rather tedious process, are usually necessary to assess this compounding effect. A one-step method, referred to as the moment magnifier method, is more widely used due to its simpler form and its more direct application.

The equation of the moment magnifier method is similar to that used in reinforced concrete beam-column design. It requires that the wall sections be designed to resist a combination of the factored axial load, P_f, and the magnified total factored moment, M_f, which is obtained from the primary moment, M_p, by applying a moment magnifier:

$$M_f = M_p \frac{C_m}{1 - P_f / P_{cr}} \tag{2.21}$$

where $1/(1-P_f/P_{cr})$ is the magnifier initially derived from elastic beam-column analysis. C_m, an equivalent moment conversion factor, is expressed as $0.6+0.4M_1/M_2$, and M_1 and M_2 are the lesser and greater end moments, respectively on a span. Since the moment magnifier method applies strictly only for uniform moment over a member, the coefficient, C_m, essentially converts the actual moment distribution to an equivalent uniform moment. P_f is the factored axial load and P_{cr} is the critical buckling load determined as follows:

$$P_{cr} = \frac{\pi^2 EI}{(kh)^2} \tag{2.22}$$

where EI is the flexural rigidity of the member at the time of failure and kh is the effective height of the member.

Both the load-displacement method and the moment magnifier method require an accurate evaluation of the flexural rigidity, a parameter affected by material nonlinearity, stress level, cracking, and creep. The creep effect is simply considered in the code by

applying a reduction factor $1/(1+0.5\beta_d)$ to proposed effective flexural rigidity $(EI)_{eff}$. Since the creep effect is outside the scope of this research, the following discussion assumes only short term loading is concerned. In addition, an overall reduction factor φ_e of 0.75 is also applied to code $(EI)_{eff}$ values to account for the random characteristics of masonry construction. In the laboratory environment however, testing conditions are well-controlled and therefore the reduction factor is not applied in the experimental results analysis in Chapter V.

The CSA Standard S304.1-M94 (1994) and the more recent CSA S304.1-M04 (2004) recommend the following equations for calculating masonry wall flexural rigidity $(EI)_{eff}$

(1) For plain and hollow concrete masonry walls

$$(EI)_{eff} = 0.40E_m I_0 \tag{2.23}$$

E_m is the modulus of elasticity taken as $850 f'_m$, where f'_m is the ultimate compressive stress of masonry. I_0 is the uncracked moment of inertia of the effective cross-sectional area.

(2) For reinforced masonry walls

$$(EI)_{eff} = E_m\left(0.25I_0 - (0.25I_0 - I_{cr})\left(\frac{e-e_k}{2e_k}\right)\right) \tag{2.24}$$

$$\text{and } E_m I_{cr} \le (EI)_{eff} \le 0.25E_m I_0$$

where I_{cr} is the moment of inertia of the cracked section ignoring axial load effects, e is the virtual eccentricity and e_k is the kern eccentricity of the effective cross-sectional area.

Although the proposed equations are simple and easy to apply, they do not provide satisfactory correlation with test data. The available literature has shown various degrees of disparity between experimental results obtained for a wide range of wall geometric characteristics and loading conditions and code values. It is noted that the $(EI)_{eff}$ value

calculated from the equations is intended for the flexural rigidity at the point where moment is maximum. Thus, it is questionable to use this effective flexural rigidity for the entire length of a wall which, in general, will develop variable depths and extents of cracking along its height. It suggests that the current design guidelines do not take into account the higher flexural rigidity inherent in walls which fail primarily by compression with only partial cracking of wall sections. In addition, for walls subjected to a symmetric single curvature bending, it is reasonable to assume that the maximum moment occurs at the mid-height of the wall. For walls subjected to asymmetric single curvature bending or reverse curvature bending, C_m is used to convert the non-uniform moment along the height of the member to an equivalent uniform moment whose location is supposed to be where the maximum lateral deflection occurs. Being empirical in nature, the equation of C_m was based on research carried out for concrete and steel compression member, and may not be directly transferable to masonry structures.

Experimental results obtained by Liu (2002) on reinforced masonry walls under combined axial and lateral loading showed that the Canadian masonry code CSA S304.1-M94 tends to underestimate $(EI)_{eff}$ values for walls that failing predominantly by compression or combined compression and tension. This underestimation is not as significant when the failure is tension controlled. It was also concluded that slenderness ratio has an effect on both wall capacity and effective flexural rigidity, where the effective flexural rigidity increases with an increase of the slenderness ratio. However, this effect is not recognized in the code equations.

Previous research on walls and columns under eccentric axial loading dealt mainly with single curvature bending. Although frequently encountered in practice, walls under either asymmetric single curvature or reverse curvature bending have received much less research attention, which has resulted in little available experimental data reported in the

literature. Although unified EI_{eff} equations are suggested in the code for the design of walls regardless of loading conditions, the validity of using the equations developed and calibrated based on results for walls subjected to symmetrical single curvature bending to walls subjected to asymmetrical single or reverse curvature bending requires further investigation.

Based on these observations, the gathering of additional information on the determination of appropriate values of $(EI)_{eff}$ and buckling capacity under varying load applications is justified.

CHAPTER III EXPERIMENTAL PROGRAM

3.1. Introduction

The experimental program consisted of two main parts including auxiliary tests and large-scale wall tests. Auxiliary test program were performed to determine the mechanical properties of masonry prisms and masonry components including mortar, unit, grout and reinforcement used throughout this experimental program. The large-scale wall test program involved the evaluation of the behavior of ten partially grouted reinforced concrete masonry walls subjected to various end moment conditions. Various combinations of end eccentricity of the applied load, generating symmetrical single curvature bending, asymmetrical single curvature bending, and reverse curvature bending were included. Detailed descriptions of the experimental set-up, wall specimens, testing procedures and auxiliary test and results are given in the following sections.

3.2 Description of Wall Tests

3.2.1 Fabrication of wall specimens

Ten partially grouted reinforced concrete masonry wall specimens were built with nominal dimensions of 2400 mm high by 800 mm long by 150 mm thick using standard 400×200×150 mm concrete blocks. All walls were constructed in running bond by an experienced mason using techniques typical of good workmanship and supervision. Figure 3.1 shows a wall specimen under construction. Each course contained either two standard stretcher blocks, or one standard stretcher block in the middle and two half corner blocks at two ends. Ready-mix type S mortar was used for building wall specimens and corresponding prisms. The bed and head joint mortar was applied only to the face shells as in common industry practice. No.9 ASWG ladder type joint

reinforcement was placed on alternate courses in each wall at a spacing of 400 mm center to center to control the mortar shrinkage.

Figure 3.1 Reinforced masonry walls under construction

As a common industry practice, mortar mixed on site was also used for grout with additional water added to facilitate the free flow of grout during the pouring of the cells. At the center of the two outer cells of each wall specimen was vertically reinforced with one 10M bar. To ensure that the rebar remained at the center of the cells, a full mortar bed was first laid on the floor and a hole was formed in the mortar bed at the intended locations of the rebars. When the wall specimen was built to a height of six courses, the

rebar was inserted in the vertically aligned cells with the bottom end inside the hole formed in the hardened mortar. At the top of the six-course masonry wall, a wire clip was used to hold the centered rebar in place while the grout was placed in the cell and rodded for compaction. The remaining six courses were then laid and grouted in a similar manner. The pattern of grout and reinforcement for wall specimens is illustrated in Figure 3.2.

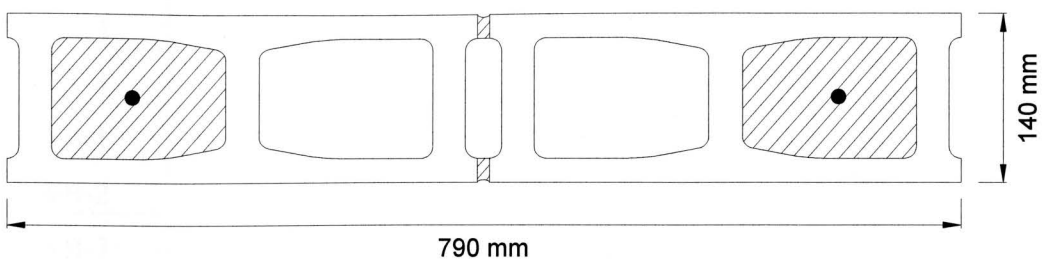

Figure 3.2 Cross-sectional configuration of wall specimens

The wall specimens were moist cured for 7 days after erection, followed by air-curing in the laboratory environment at temperature conditions ranging from 15 to 25 degrees and a relative humidity ranging from 40 per cent to 60 per cent. The wall specimens were cured at least 28 days before the testing commenced.

3.2.2 Description of wall specimens

A general description of wall specimens is presented in Table 3.1 for the three series of specimens tested in this program. All specimens were tested under eccentric compressive loading. Different end moment loading conditions were created by applying eccentricity of the compressive load at various locations on the ends of the wall. Eccentricity ratio (e/t) of 1/6, 1/4 and 1/3 were selected for this study. Four specimens were tested in WA series under symmetrical single curvature bending with e_1/e_2=1.0. WB series included three specimens subjected to asymmetrical single curvature bending with e_1/e_2=0.0 and WC

series involved the testing of 3 specimens subjected to reverse curvature bending with e_1/e_2=-1.0. Loading conditions of the specimens are shown schematically in Figure 3.3.

Table 3.1 Description of wall specimens

Specimen	Grouted cores	Reinforcement	e_1/t	e_2/t	e_1/e_2
WA-1	2	2-10M	1/6	1/6	1.0
WA-2	2	2-10M	1/4	1/4	1.0
WA-3	2	2-10M	1/3	1/3	1.0
WA-4	2	2-10M	1/3	1/3	1.0
WB-1	2	2-10M	0	1/6	0.0
WB-2	2	2-10M	0	1/4	0.0
WB-3	2	2-10M	0	1/3	0.0
WC-1	2	2-10M	-1/6	1/6	-1.0
WC-2	2	2-10M	-1/4	1/4	-1.0
WC-3	2	2-10M	-1/3	1/3	-1.0

3.2.3 Test set-up

3.2.3.1 Testing frame

The test set-up for wall tests is shown in Figure 3.4. The testing frame, with a design capacity of 2100 kN, consists of two individual frames connected together by welding a steel plate of 31 mm thickness at the bottom flange of cross-beams. The W310×86 supporting columns were bolted to the strong floor using two 48 mm and two 56 mm steel rod bolts through a 900×500×40 mm base plate. The W610×241 steel cross beams were simply connected to the supporting column flanges using six 24 mm bolts through L127×127×13 double clip angles. The webs of the cross beams were stiffened by four C100×11 vertical stiffeners with a length of 238 mm spaced at 600 mm on center.

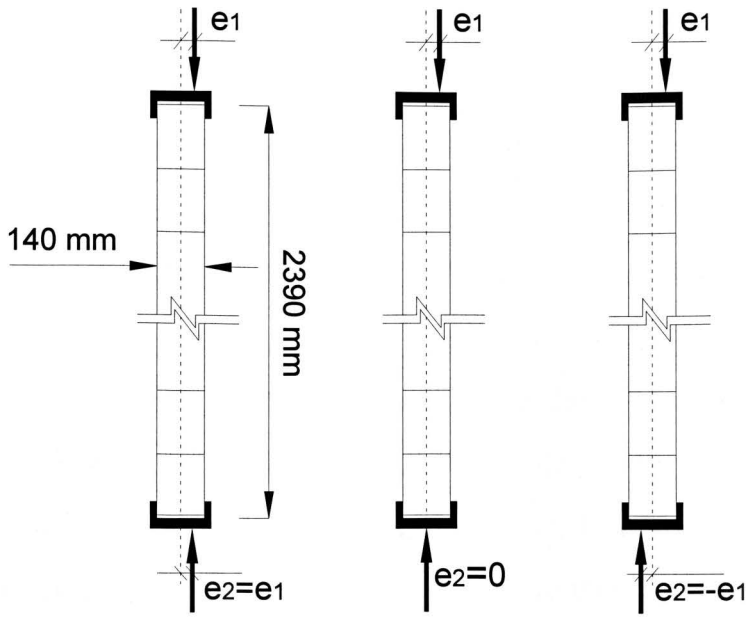

(a) WA walls (b) WB walls (c) WC walls

Figure 3.3 Loading conditions of the three series of wall specimens

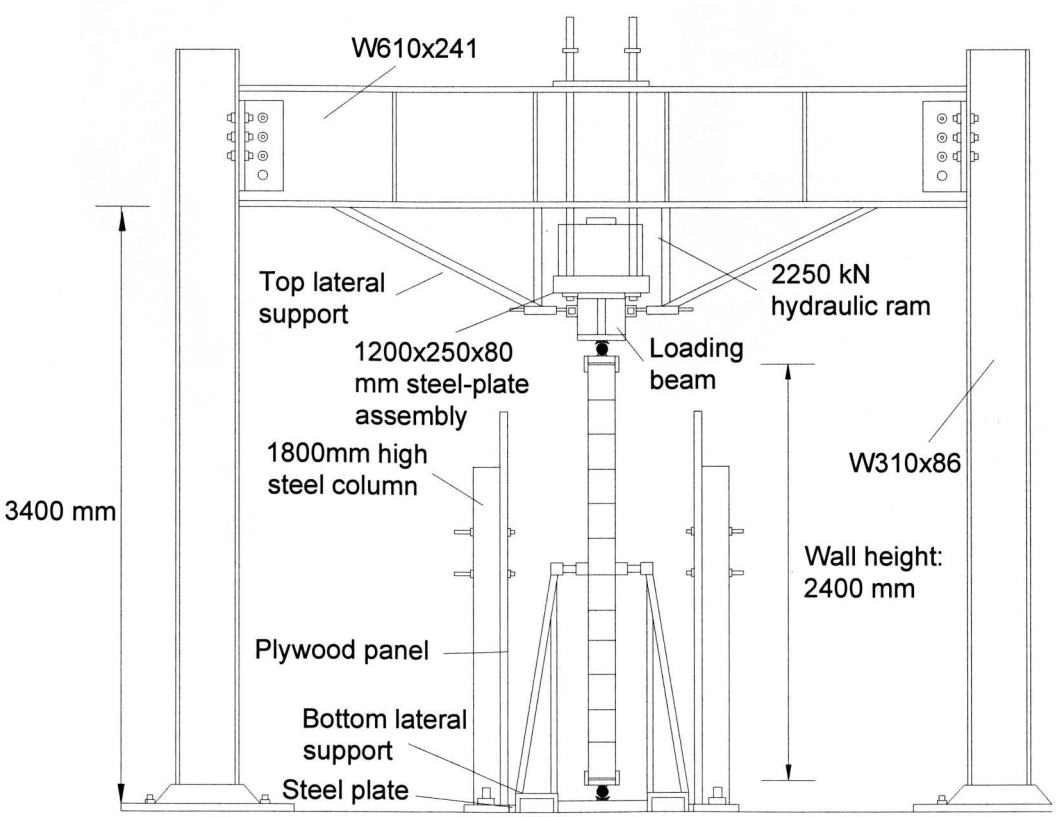

Figure 3.4 Testing frame

3.2.3.2 Support conditions

Pinned-pinned support conditions were adopted in all wall tests. Key components of a pinned support at bottom of the specimen included a 60 mm diameter round bar welded to a channel-shaped steel-plate assembly used to hold the specimen ends and a half-pipe welded onto a plate positioned and fixed to the strong floor. The half-pipe was formed by symmetrically cutting a 60 mm diameter steel pipe in the longitudinal direction. The channel and round bar assembly were then placed into the half-pipe to provide a pin support. A similar arrangement was made for the top pinned support. To prevent sliding at wall ends inside the built-up channel, four holes were drilled on one flange of each channel along its length, and bolts were then tightened against the wall surface during testing. Figure 3.5 shows a close-up view of the fabricated steel channel with 60 mm diameter round bar attached.

Figure 3.5 Close-up view of roller support

A complete roller support at the bottom of the specimen is illustrated in Figure 3.6.

Varying eccentricities used in the test were achieved by simply welding the round steel

bar to the corresponding positions indicated by the eccentricity versus thickness ratio.

3.2.3.3 Compression loading arrangement

Vertical compressive loading was applied to each wall specimen using a 2250 kN hydraulic ram. Details of the vertical loading arrangement are shown in Figure 3.7. The hydraulic ram was fastened to a three-plate assembly measuring 1200×250×80 mm using four bolts. Prior to testing, the plate assembly and ram were held in position above the wall using four long steel rods fastened with nuts on the top flanges of the cross beams. During the test, the nuts were loosened to allow the ram to travel freely in the vertical direction. A 1200 mm long loading beam of W310×86 section was used to transfer the loading to the top of the wall specimen. The web of the loading beam was stiffened by welding three pairs of C100×11channel against either side of the web.

Figure 3.6 Pinned support configuration

Figure 3.7 Loading arrangement and top bracing for wall test

3.2.3.4 Lateral support

In order to counteract the lateral shear force at wall ends caused by non-uniform bending in reverse curvature and asymmetrical single curvature wall tests, the wall specimens were laterally braced at the top as shown in Figure 3.7 and at the bottom as shown in Figure 3.8. Two 1000 mm long steel HSS sections were held against both sides of the loading beam, which allowed vertical movement but prevented the lateral movement of the beam. Enough traveling distance was left between the lateral bracing steel HSS sections and the top flanges of the blue beam. The wall rested directly on the bottom support assembly as shown in Figure 3.8. This assembly consisted of a 1000×800×50 mm steel plate with two standard C250×45 channels welded on either side. Two 1000 mm long steel HSS sections were held against the mid-height of the wall at either side to provide lateral bracing before each test. The steel sections were designed as removable before each testing, which allows the wall deflect laterally freely during testing. These sections were supported in position by two steel supporting frames attached to the base assembly as shown in Figure 3.8. Long steel plates were squeezed in-between the bases

of the bottom support assembly and the vertical columns to prevent lateral slide of the wall specimen at bottom.

Two 1800 mm high steel columns with a clear space of 1400 mm were bolted to the strong floor of the laboratory. Two plywood panels with dimensions of 1600×2400×20 mm were attached to those two columns at either side of the wall to limit the impact of possible collapse of walls at failure acting as stoppers. A wire cage was also used to confine the failed wall and falling debris.

Figure 3.8 Lateral support at bottom of the specimen

3.2.4 Wall transportation

To transport the wall specimen from the fabrication area to the test area, each wall

specimen was tightly clamped at the mid-height by two structural timber sections bolted together and used for lifting purpose. Two steel slings were attached to the clamping system at each end, and an overhead crane was used to lift and carry the wall specimens from the fabrication area to the front of the testing frame. A forklift was then used to carry the wall and the support assembly into the testing position as shown in Figure 3.9.

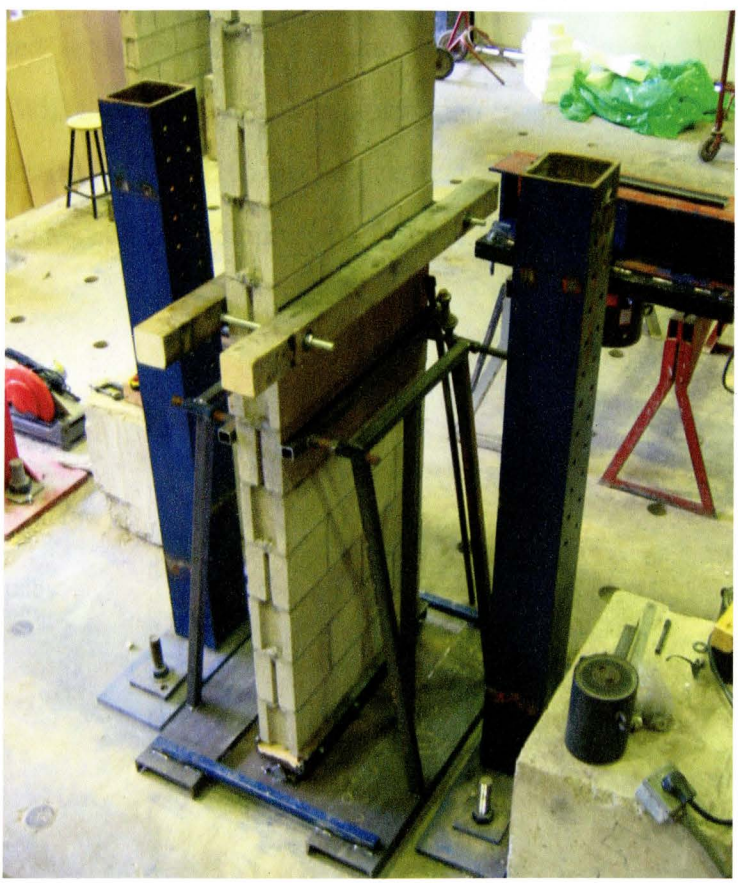

Figure 3.9 Transportation of wall specimens

3.2.5 Instrumentation and data acquisition

Vertical deformations and lateral deflections were measured using linear variable differential transducers (LVDT). Deformations were measured and used to calculate the vertical strains on the tension and compression faces of the walls. The details of

instrumentation for the majority of specimens are shown in Figure 3.10. Vertical deformation was measured within a predetermined gauge length at two locations of 400 mm apart to ensure that the vertical deformations were measured consistently along the length of the specimen. Screws were drilled on the faceshell of the wall at top of the gauge length and small pulleys were mounted on the bottom of the gauge length. Nylon monofilament lines were used to connect from screw through the pulleys to the LVDTs which were attached to an independent frame outside the plywood panels to avoid damage at failure. While only the vertical deformation measurement on one side of the specimens is shown in Figure 3.10, similar vertical deformation measurements were instrumented on both tension and compression faces of the specimens.

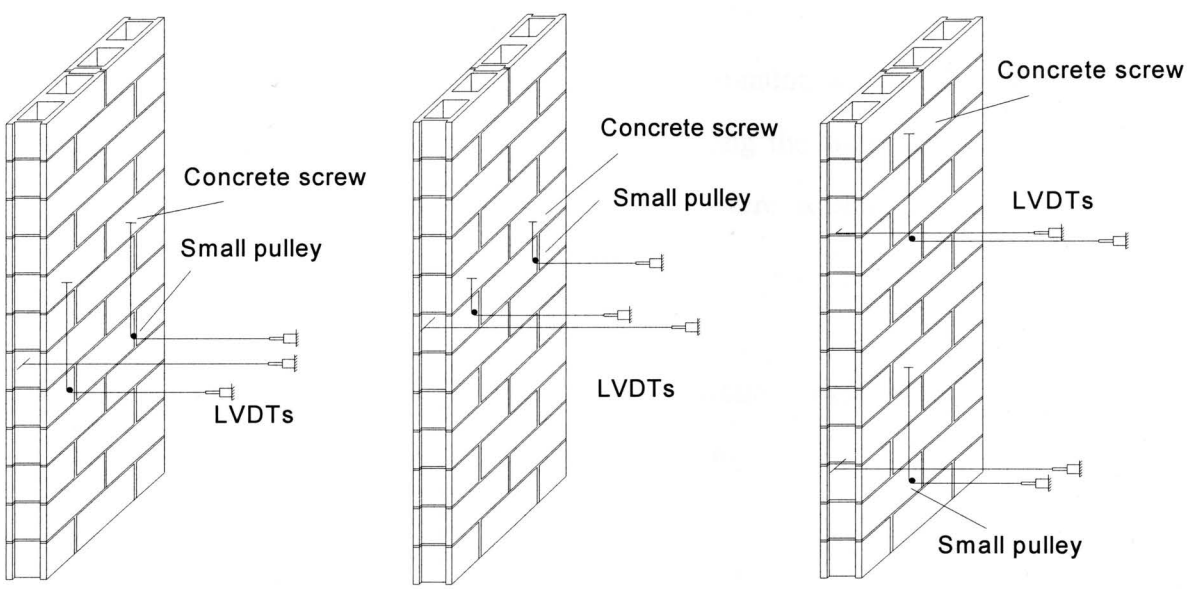

(a) WA walls (b) WB walls (c) WC walls

Figure 3.10 Instrumentation of the majority of wall specimens

The gauges wer e placed at the location theoretically determined point of maximum lateral deflections. For walls subjected to symmetrical single curvature bending, lateral deflections were measured at mid-height of each specimen and vertical deformations

were measured at the mid-height with a nominal gauge length of 600 mm. For reverse curvature bending, maximum lateral deflection occurred in the vicinity of the mortar joint between the 3rd and 4th course from the top or bottom of a wall. Vertical deformations were measured at the corresponding locations with a nominal gauge length of 600 mm. Lateral deflections were measured at the mortar joints between the 3rd and 4th courses and the 9th and 10th courses. The predicted maximum lateral deflection location for the asymmetrical single curvature bending wall was determined to be at mortar joint between the 7th and 8th courses from the bottom. LVDTs measuring the lateral deflections were attached to the mortar joints between courses. A gauge length of 200 mm was used in the axial deformation measurements for the asymmetrical single curvature bending walls.

For specimens WA-1 and WC-1, a different instrumentation scheme was adopted where lateral deflections were measured at 7 locations along the wall height as indicated in Figure 3.11. The locations for the seven LVDTs were selected so as to obtain the complete deflected shape of the wall.

Vertical loads, vertical deformations and lateral deflections were measured and recorded by an electronic multi-channel data acquisition system.

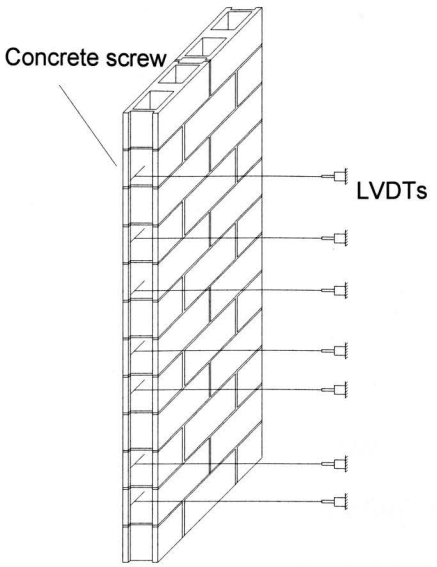

Figure 3.11 Instrumentation of specimens WA-1 and WC-1

3.2.6 Test procedure

Fiberboard capping placed between the loading supports and the ends of a specimen was used to eliminate stress concentrations and to enhance uniformity. The half round pipes used as half of the load eccentricity system were greased before each test to assist free rotation of the eccentrically loaded walls which were centered and vertically aligned using a laser level. Once the wall was placed in the testing position, the loading apparatus was slowly lowered using a crane until full contact with the wall specimen was achieved. This hold the specimens in place ready for testing.

Before testing, each specimen was loaded cyclingly twice using approximately ten per cent of the predicted ultimate load to ensure that the specimen and instrumentation were properly positioned. During a typical test, the vertical load was applied gradually at a rate of about 65 kN per minute until failure occurred. Cracking, and crack locations and corresponding load levels as well as failure modes were noted for each specimen. Failure

and ultimate loads were considered to have occurred when the specimens displayed large lateral deflections at decreasing axial loads.

3.3 Auxiliary Tests

3.3.1. Masonry materials

In this experimental program, standard 140 mm normal weight stretcher and corner blocks, ready-mix type S mortar, 10M deformed reinforcing bars and standard No. 9 ASWG ladder type joint reinforcement were used. Concrete half-blocks used to build the masonry walls were obtained by cutting masonry corner blocks along the centerlines. Auxiliary tests as described below were conducted to determine mechanical properties of these materials and to maintain quality control.

1. Measured dimensions

Dimensions and net and gross areas were measured for both stretcher and corner blocks used in the experiments. For each type of block, 5 units were randomly selected in the consignment and measured. Net to gross area ratios were obtained according to the measurements. Procedures for determining the dimensions and net and gross areas conformed to ASTM C 140-02a (2004).

2. Mechanical properties

Five hollow block units selected randomly from the shipment were tested to determine the compressive strength of the units. Due to space and resource limitations, five grout prisms measuring 150×75×75 mm and six 50 mm mortar cubes were cast for wall and prism specimens. A consistent mix specification was therefore followed for each batch of grout and mortar mixed on site to reduce the level of discrepancy caused by construction.

Grout prisms and mortar cubes were cured to determine ultimate compressive strength according to ASTM C1019-02 (2004) and ASTM C109 (2004), respectively. Three reinforcement coupons were cut randomly from the rebar shipment to determine the yield and ultimate strengths of the reinforcement according to ASTM A 370-02 (2004).

3.3.2. Prism test

To evaluate the material strength and modulus of wall specimens which were partially grouted, six 3-high block prisms including three hollow prisms and three fully grouted prisms were constructed and tested according to ASTM C1314-02a (2004) to determine the masonry compressive strength, f'_m, modulus of elasticity, E_m, and the stress-strain relationship of masonry in compression. For the grouted prisms, the same batch of grout for filling the cores of wall specimens was used. Each cell in the grouted prism was filled to one-half the depth and rodded 25 times, and the remaining upper half filled and similarly rodded without disturbing the lower half. Prisms were constructed at the same time as the corresponding wall specimens, and were allowed to cure in the laboratory at least 28 days under the same condition as the walls built with the same mortar and grout batch. Prisms and walls were tested as nearly as possible at the same age.

Flat end support conditions were adopted for prism test according to ASTM standard. To obtain the stress-strain relationship of masonry in compression, vertical deformation within a predetermined gauge length of 400 mm was measured on both faces of the masonry prism using a LVDT arrangement similar to that described for wall test. Lateral deflection at mid-height of the prism was also measured using an additional LVDT. The test set-up and instrumentation are shown in Figure 3.12.

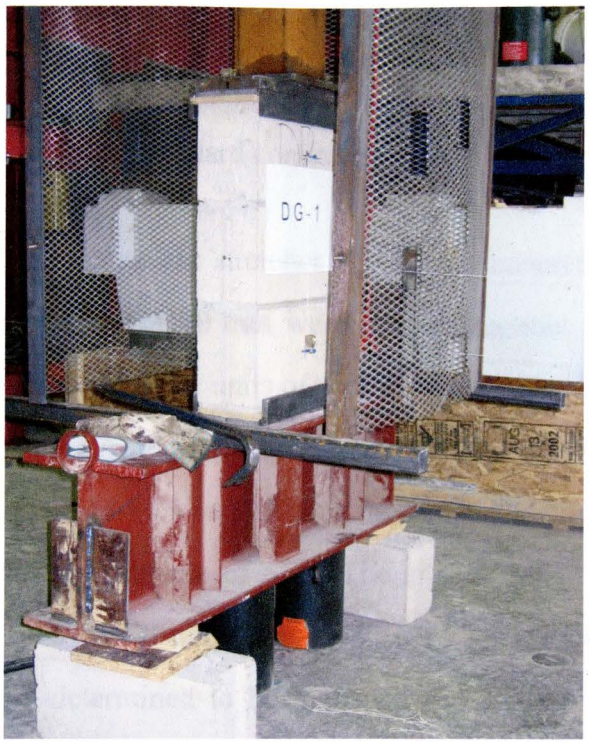

Figure 3.12 Prism test

Prisms were soft-capped with 10 mm thick fiberboard as for all wall specimens. The load was monotonically applied with a loading rate adjusted so that the maximum load would be reached in about three minutes. Failure occurred when the specimen displayed large vertical and diagonal cracks through the web and faceshell with an accompanying drop in the applied axial loading. The compressive strength, f'_m, for each specimen was calculated using the measured axial load divided by the effective net area of the prism cross-section.

3.4. Results of Auxiliary Tests

3.4.1. Measured dimensions of standard concrete blocks

Autoclaved, standard normal weight stretcher and corner concrete masonry units with nominal dimensions of 400×200×150 mm were used throughout the test program. The mean of measured dimensions of five units of each type are demonstrated in Figure 3.13. From the measurements, the average net cross-sectional area of the stretcher block was determined to be 29924 mm², which resulted in a mean net to gross area ratio of 0.55 and an average per cent solid by volume of 56.5. The average cross-sectional area of the standard corner block was 33660 mm². The mean net to gross area ratio and per cent solid were subsequently determined to be 0.62 and 63.2, respectively. The measured dimensions were used in the analysis presented in the following chapters.

3.4.2. Mechanical properties

3.4.2.1. Concrete masonry blocks

Five randomly selected units were soft-capped and tested under axial compression in a Maruto compression machine of 2000 kN capacity. Block units were centered under the loading head of the compression machine and loaded to ultimate. Axial loads were measured and recorded and then divided by the net cross-sectional areas obtained as described before to calculate the compressive stresses. The mean ultimate compressive strength of the standard blocks was 25.17 MPa with a C.O.V of 11.7 per cent.

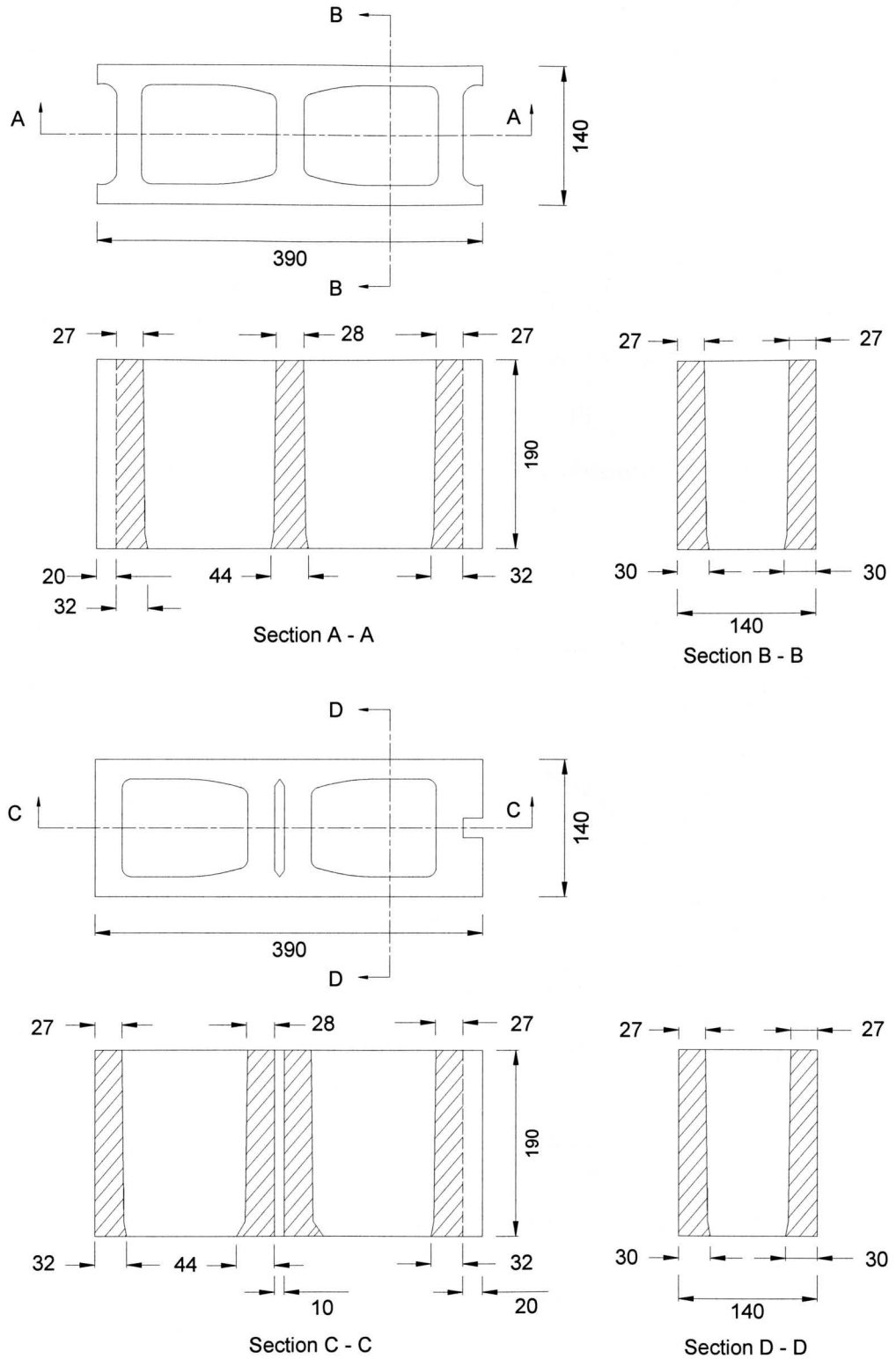

Figure 3.13 Measured dimensions of stretcher and corner blocks (mm)

3.4.2.2. Mortar

Type S masonry cement was used as the cementious material, which was mixed with masonry sand provided by local suppliers to obtain type S mortar for building all the test specimens in the program. Six 50 mm mortar cubes were cast in non-absorbent moulds during the construction of the assemblages. The cubes were cured for 24 hours in the moulds and stripped and immersed in lime water for curing to approximately the same age as the corresponding assemblages according to ASTM C109 (2004). A typical stress-train curve in mortar cube tests is shown in Figure 3.14. The mean value of compressive strength of the mortar cubes was then obtained to be 15.26 MPa with a C.O.V of 9.1 per cent.

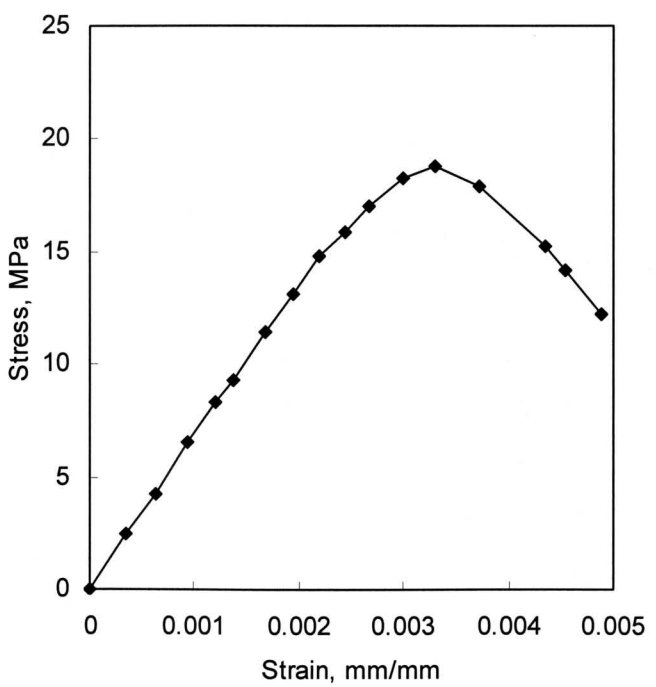

Figure 3.14 Typical stress vs. strain curve in mortar cube tests

3.4.2.3. Grout

Grout used in this program was made using type S masonry cement, masonry sand, and

water. The water/cement ratio was adjusted to assure a high slump grout suitable for ease of pouring.

Five grout prisms capped with sulfur on both ends were tested using a 250 kN capacity Instron compression machine for compressive strength according to ASTM C 1019-02 (2004). During testing, vertical deformations and axial loads were measured and recorded. Due to the small size of grout prisms, vertical deformations were measured from the traveling of the loading head of the compression machine. The mean compressive strength of the grout prisms was 18.83 MPa with a C.O.V of 8.3 per cent. A typical stress-strain curve for a grout specimen is shown in Figure 3.15.

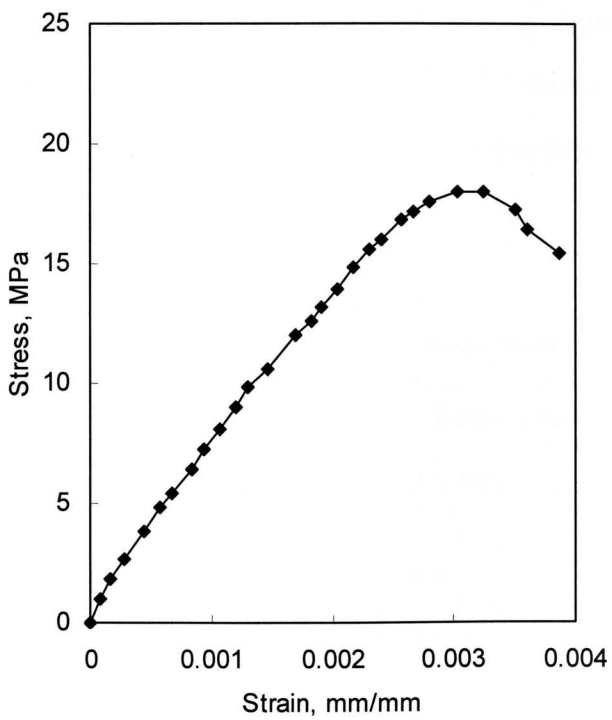

Figure 3.15 Typical stress vs. strain curve in grout prism tests

3.4.2.4. Prism test

Results for 6 prism specimens tested in axial compression are presented in Table 3.2.

While compressive strength was calculated simply using axial ultimate load divided by the effective net area, stress vs. strain curves were used to determine the E_m values as specified in Clause 8.3.1.4 of CSA S304.1-M04. Typical stress vs. strain curves for hollow prisms and fully grouted prisms are shown in Figure 3.16 and 3.17, respectively. The f'_m and E_m values for hollow prisms were determined to be 21.1 MPa and 16645 MPa and 14.5 MPa and 13112 MPa for fully grouted prisms according to Clause 9.2 of CSA S304.1-M04. The average of mean f'_m values of 17.8 MPa and mean value of E_m of 14879 MPa were used as the compressive strength and modulus of elasticity of masonry walls in the following analysis. The prism test results showed good consistency and the coefficient of variations of which as shown in Table 3.2 are well below the variation limit of 15% specified in CSA S304.1-M04. Typical vertical splitting occurred through the webs of the hollow prisms and the failure was complete as shown in Figure 3.18. A typical failure mode observed in the fully grout prism tests is shown in Figure 3.19 where vertical splitting through the webs was observed while some portion of grout remained intact.

Table 3.2 Results of prism tests

Specimen	Hollow prism		Fully grouted prism	
	f'_m (MPa)	E_m (MPa)	f'_m (MPa)	E_m (MPa)
1	22.0	16443	15.0	12733
2	24.2	17263	16.6	13120
3	22.4	16229	17.3	13483
Mean	21.1	16645	14.5	13112
C.O.V	5%	3.3%	7.2%	3%

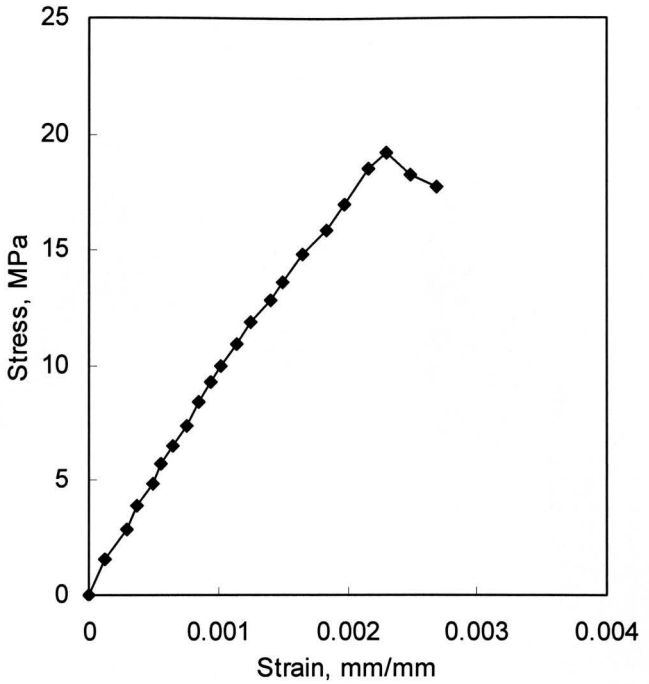

Figure 3.16 Stress vs. strain curve for 3-high hollow prism

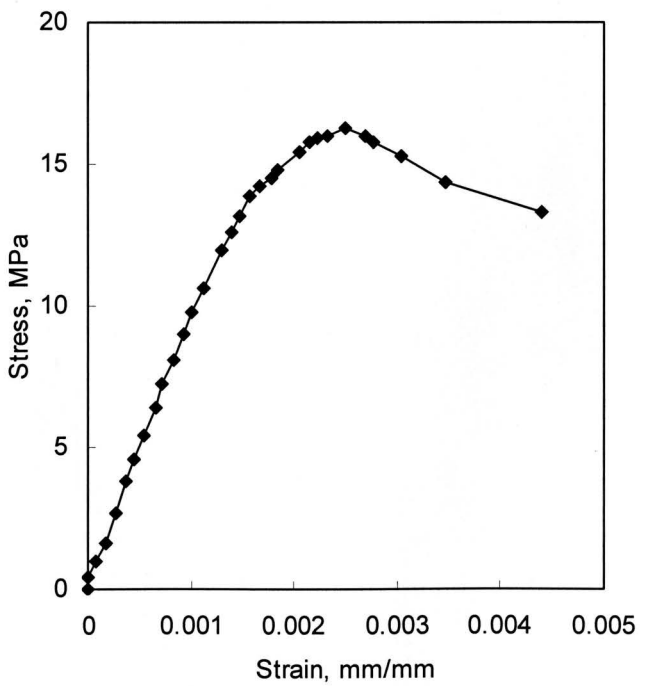

Figure 3.17 Stress vs. strain curve for 3-high fully grouted prism

Figure 3.18 Web splitting in 3-high hollow prism test

Figure 3.19 Failure mode of 3-high fully grouted prism test

3.4.2.5. Vertical reinforcement

Three 200 mm long 10M rebar coupons were tested for ultimate and yield stresses in a 100 kN capacity Instron machine under uniaxial tension according to ASTM A 370-02 (2004). A typical stress-strain curve for reinforcement steel bars is shown in Fig 3.19. The average yield stress f_y was 447 MPa and the average modulus of elasticity was 188688 MPa. The average ultimate stress, f_u, was 743 MPa.

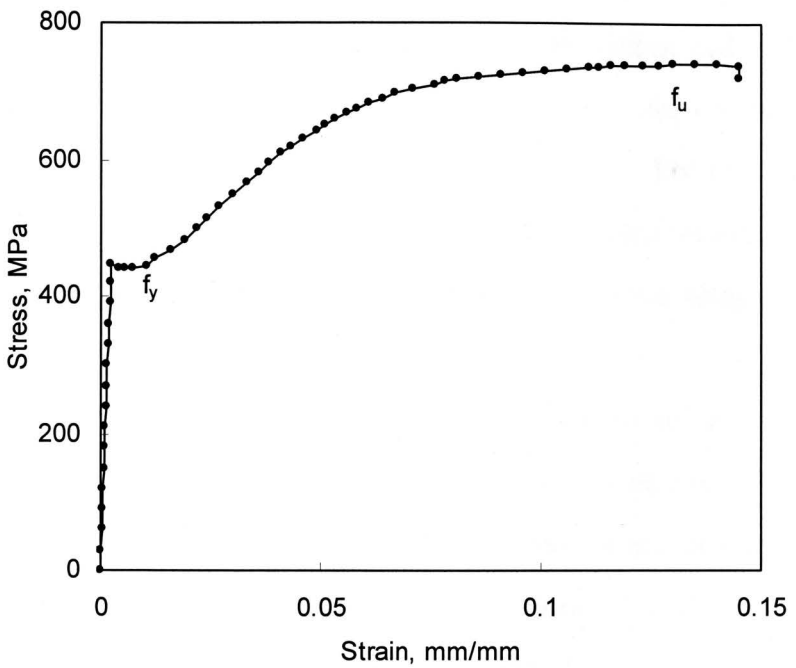

Figure 3.20 Typical stress-strain curve for vertical reinforcement

CHAPTER IV LARGE-SCALE WALL TEST RESULTS

4.1 Axial Load Capacity

The results of ten wall specimens tested under eccentric compressive loadings are summarized in Table 4.1, where e/t is the ratio of eccentricity to wall thickness, P_u is the ultimate axial load, Δ_u is the lateral deflection measured at P_u, and M_u is the maximum moment at the location of lateral deflection measurement calculated as $P_u(e + \Delta_u)$. The slenderness ratio, h/t, of all specimens is 17.1. Two specimens WA-3 and WA-4 in WA series under identical loading and boundary conditions were tested first to ensure that the devised test set-up was reliable for obtaining consistent test results. The variation of ultimate loads of specimen WA-3 of 474.3 kN and specimen WA-4 of 526.8 kN is approximately 11 per cent, which is considered acceptable in masonry practice. As a result, the following tests were conducted using one specimen for each loading condition.

As seen in the table, as eccentricity ratio increases, the wall capacity for specimens in WA series and WC series decreases. The reduction of wall capacity is also observed between specimens WB-2 and WB-3 in WB series. However, specimen WB-1 tested at eccentricity ratio of 1/6 failed at a lower load than that of WB-2. This anomalous result is attributed to a pre-existing crack on the top corner of the specimen due to construction. The decrease of wall capacity with an increase of the eccentricity ratio is further illustrated in Figure 4.1 where P_u vs. e/t curves for all three series were plotted. It appears that while the decreasing trend is evident for all three series, the rate of the decrease is most significant for WA series under symmetrical single curvature bending and followed in sequence by WB series and WC series walls. A comparison of wall capacities obtained for all three series showed that in general, specimens tested under reverse curvature bending attained greater ultimate load than those subjected to asymmetrical single curvature bending. The wall specimens tested under symmetrical single curvature bending showed the lowest capacity.

Table 4.1 Summary of large-scale wall test results

Specimen	Eccentricity e/t	End Moment Ratio e_1/e_2	Maximum Compressive Load, P_u (kN)	Deflection at P_u, Δ_u (mm)	Moment M_u (kN-m)
WA-1	1/6, 1/6	1.0	1029.3	2.03	26.1
WA-2	1/4, 1/4	1.0	894.9	4.00	34.9
WA-3	1/3, 1/3	1.0	474.3	3.05	23.6
WA-4	1/3, 1/3	1.0	526.8	4.16	26.8
WB-1	0, 1/6	0.0	1011.7	0.74	24.4
WB-2	0, 1/4	0.0	1096.8	1.67	40.2
WB-3	0, 1/3	0.0	906.5	1.63	43.8
WC-1	-1/6, 1/6	-1.0	1203.6	0.71	28.9
WC-2	-1/4, 1/4	-1.0	1124.2	1.04	40.5
WC-3	-1/3, 1/3	-1.0	1022.2	1.65	49.4

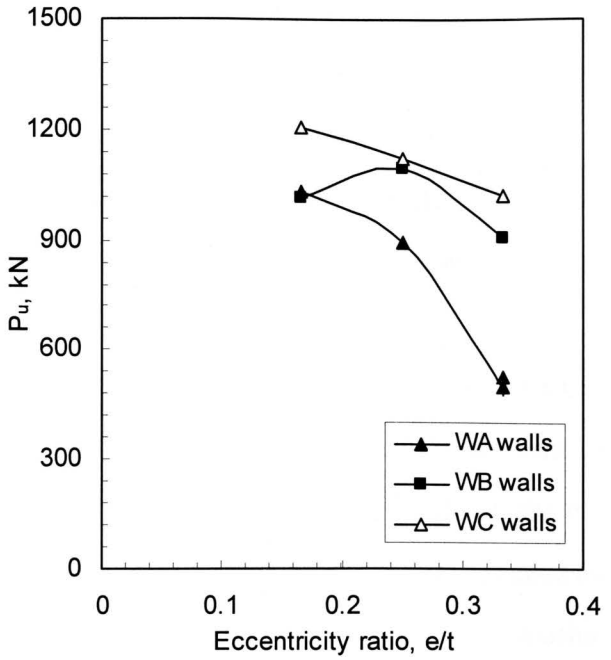

Figure 4.1 P_u vs. e/t for wall specimens in three series

4.2 Load response and failure modes

4.2.1 WA series (symmetrical single curvature bending)

Four reinforced masonry wall specimens were tested in WA series under symmetrical single curvature bending with equal load eccentricities at both ends. Two walls, WA-3 and WA-4 were tested at a load eccentricity ratio e/t equal to 1/3, and WA-1 and WA-2 were tested with load eccentricities of $t/6$ and $t/4$, respectively.

For specimen WA-1, the failure was initiated by vertical cracking in the webs and faceshells at the bottom three courses of the specimen at about 90 per cent of the ultimate load. At failure, the faceshell of the bottom 3 courses spalled off and the compressive steel buckled due to the loss of the confinement as can be seen in Figure 4.2. It is however not clear whether the steel buckling occurred at ultimate or sometime before.

The top portion of the specimen remained intact at failure of the wall. The failure location was different from that normally expected for a symmetrical single curvature bending. The greater force attracted to the bottom of the specimen was believed to be a result of friction generated in the support between the pipe and rod due to insufficient grease. The problem was corrected for the remaining tests.

A combined tension and compression failure mode was observed in specimen WA-2, which was loaded with an eccentricity of $t/4$. Up to 80 per cent of ultimate load, small tensile cracks occurred at the mortar joint one course above the mid-height mortar joint. As the applied load increased, masonry crushing on the compressive face was observed. At failure, the faceshell of the course above the mid-height mortar joint spalled off and the masonry on the compressive face was totally crushed as shown in Figure 4.3.

For specimens WA-3 and WA-4 tested under an eccentricity of $t/3$, failure was initiated by the formation of horizontal cracks along mortar joints at mid-height of wall specimens. The tensile cracks began to open up as the applied load increased. The failure was relatively ductile with an increased lateral deflection. Some crushing of masonry was also observed at the compressive face of WA-3 at failure but it was not as significant as that in specimen WA-2. However, no evident masonry crushing was observed in WA-4. A typical failure mode and a close-up view of horizontal mortar joint cracks are shown in Figure 4.4 and Figure 4.5, respectively.

Figure 4.2 Failure mode of wall specimen WA-1

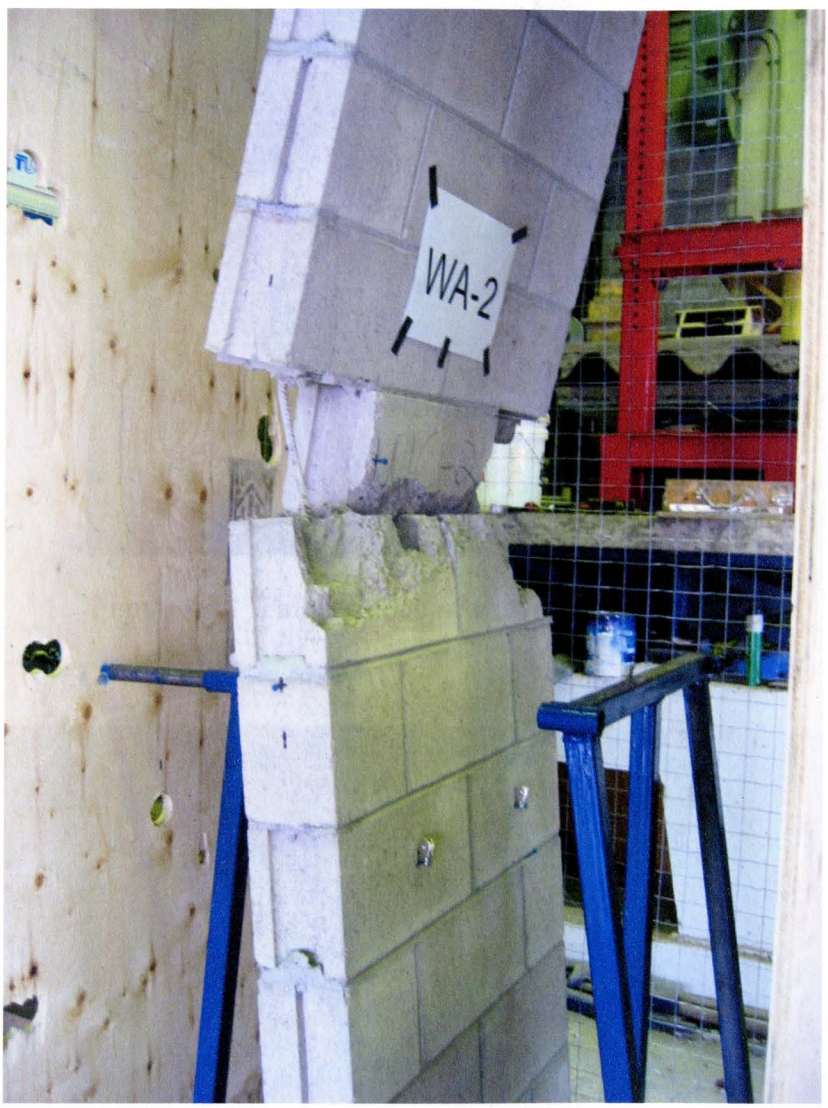

Figure 4.3 Failure mode of wall specimen WA-2

Figure 4.4 Failure mode of wall specimen WA-4

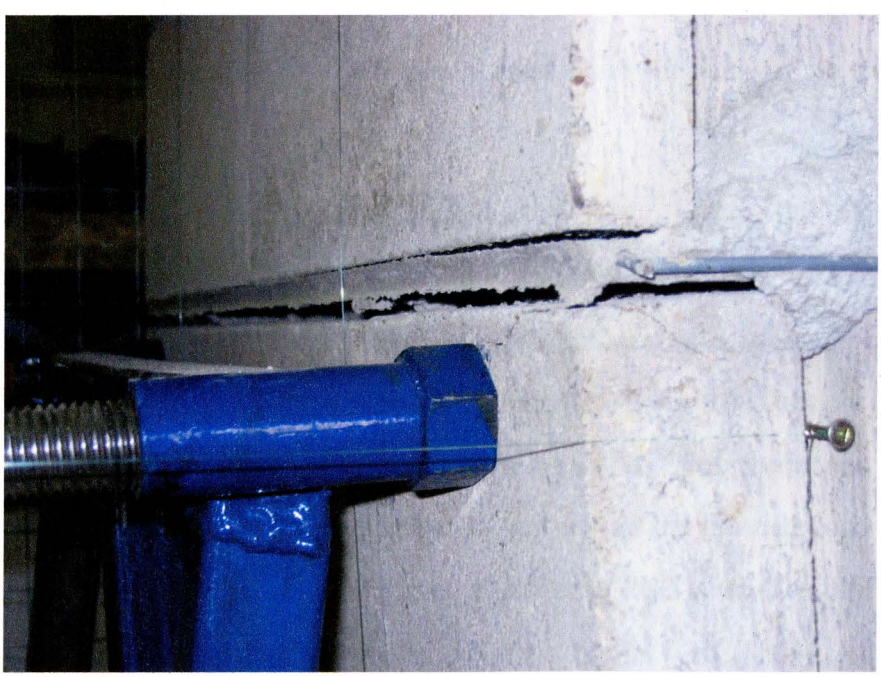

Figure 4.5 Horizontal mortar joint cracking in WA-4

For specimen WA-1, lateral deflections were measured and recorded at seven locations along the height of the wall. The lateral deflections with respect to the wall height at various load levels are shown in Figure 4.6. The curves showed that lateral deflections increased with increase of the applied load while the maximum deflection occurred at the bottom of the specimen which was consistent with the observed failure modes.

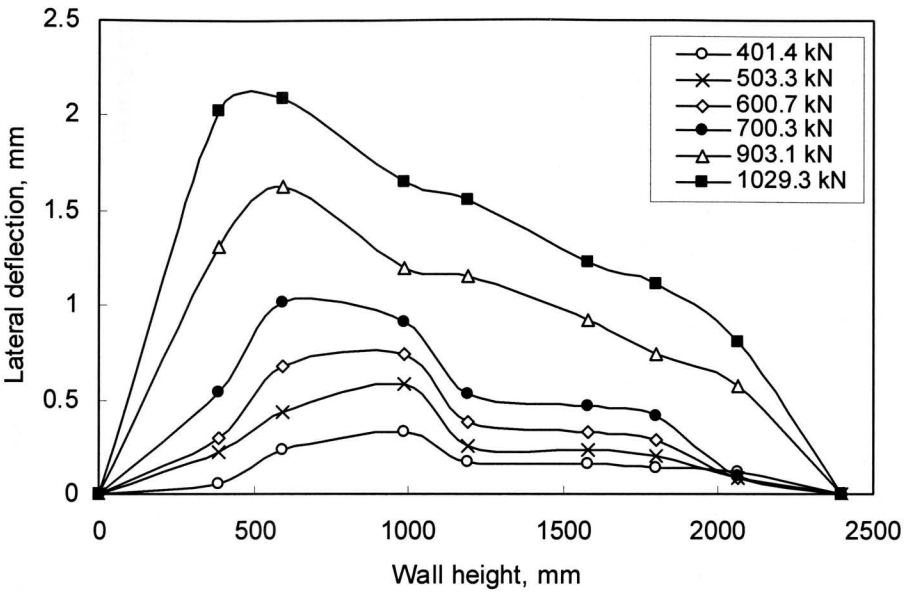

Figure 4.6 Deflected shape of wall WA-1

Vertical compressive load vs. lateral mid-height deflection curves for WA series are shown in Figure 4.7. For specimen WA-1, the linear behavior was maintained up to almost 90 per cent of the ultimate. The failure was sudden accompanied with a small deflection of less than 2 mm. The curve for specimen WA-2 remained almost linear up to 80 per cent of the ultimate load with an increased ductility. For specimens WA-3 and WA-4, the nonlinear response began at about 70 per cent of the ultimate load which was accompanied by the tensile cracking observed at a similar load level. The ultimate lateral deflection reached between 4 to 7 mm.

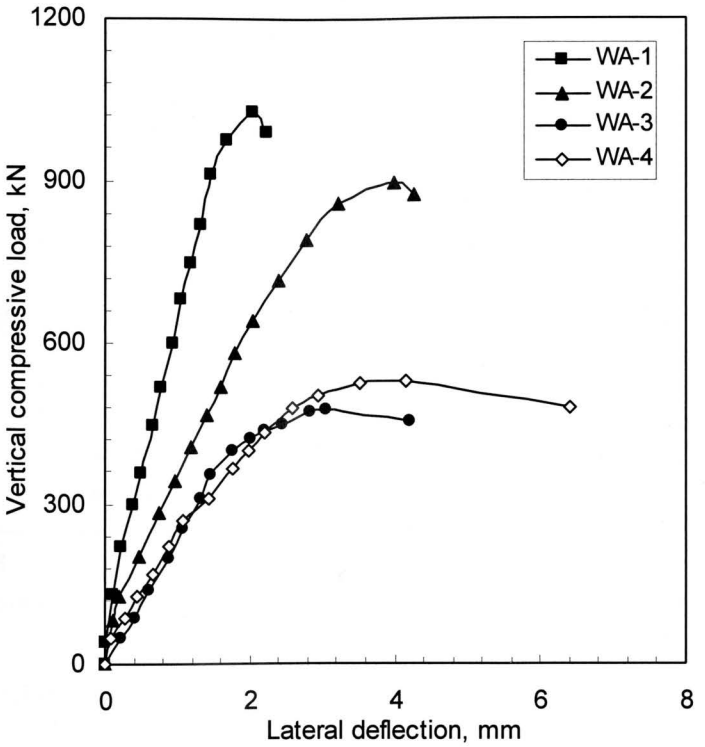

Figure 4.7 Vertical compressive load vs. lateral mid-height deflection curves for wall specimens in WA series

Figure 4.8 shows typical graphs of vertical compressive load vs. vertical deformations. Two vertical deformations of 400 mm apart along the wall length measured on the compression side of wall WA-2 are plotted in Figure 4.8 (a). The two vertical deformations measured on the tension side of wall WA-2 are shown in Figure 4.8 (b). Vertical deformation measurements for wall specimen WA-3 are shown in Figure 4.9 (a) and (b). It is evident from these curves that vertical deformation measured at different locations along the masonry wall length are consistent, which indicates that the applied load was distributed evenly over the length of the cross-section.

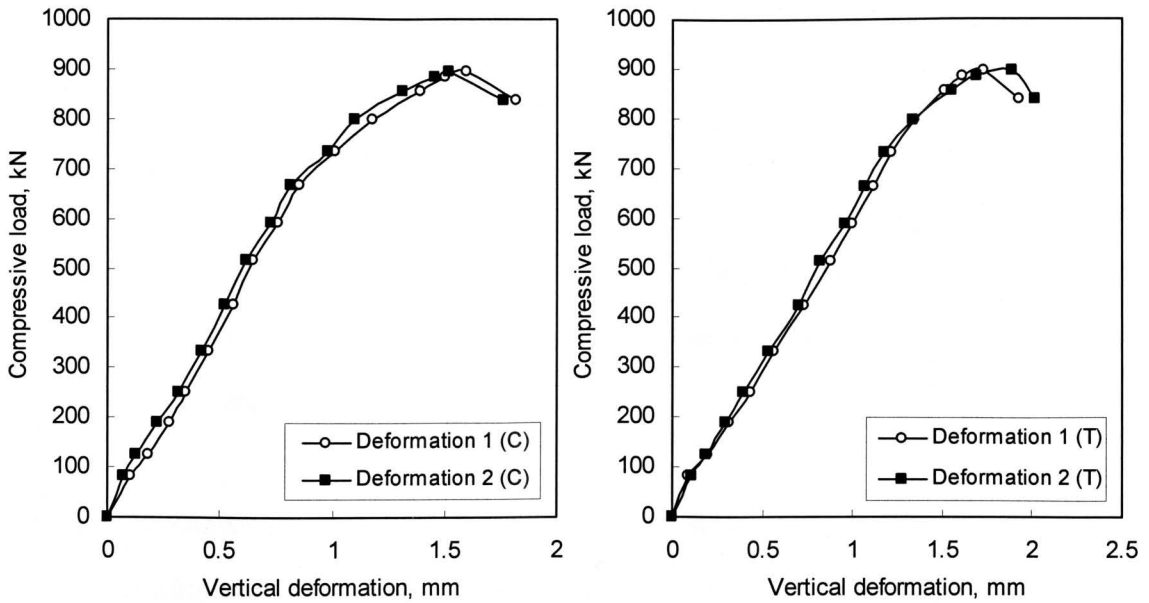

(a) Compression side deformations (b) Tension side deformations

Figure 4.8 Vertical compressive load vs. vertical deformation curves for wall WA-2

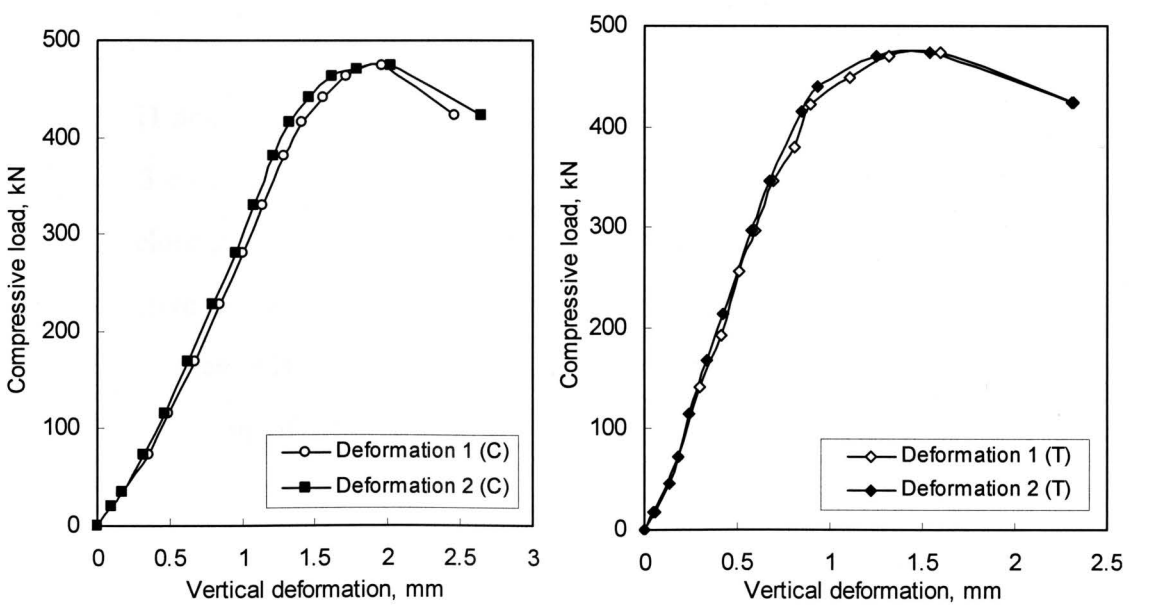

(a) Compression side deformations (b) Tension side deformations

Figure 4.9 Vertical compressive load vs. vertical deformation curves for wall WA-3

4.2.2 WB series (asymmetrical single curvature bending)

Three reinforced masonry wall specimens were tested in WB series under asymmetrical single curvature bending where compressive loading was applied eccentrically at top end of the specimen and concentrically at the bottom. Specimens WB-1, WB-2, and WB-3 were tested under load eccentricities applied at top end of the specimen equal to $t/6$, $t/4$ and $t/3$, respectively.

Figure 4.10 shows the failure mode of specimen WB-1, which was initiated by the vertical splitting cracks in two end block webs as is evident in the figure. Masonry crushing on the compressive face was also observed before failure. The failure was sudden and accompanied by the faceshell spalling and buckling of the rebar as shown in Figure 4.10. The bottom portion of the specimen remained in the test frame and visually intact.

Figures 4.11 and 4.12 show the failures of specimens WB-2 and WB-3, both of which f in the top 3 courses. The failures were explosive accompanied with a sudden release of energy. A close examination of specimen WB-2 after failure showed that a larger portion of compressive face crushed indicating the failure was predominantly compressive. In the case of specimen WB-3, horizontal cracks were observed at the second course mortar joint before spalling of the faceshell.

Figure 4.10 Failure mode of wall specimen WB-1

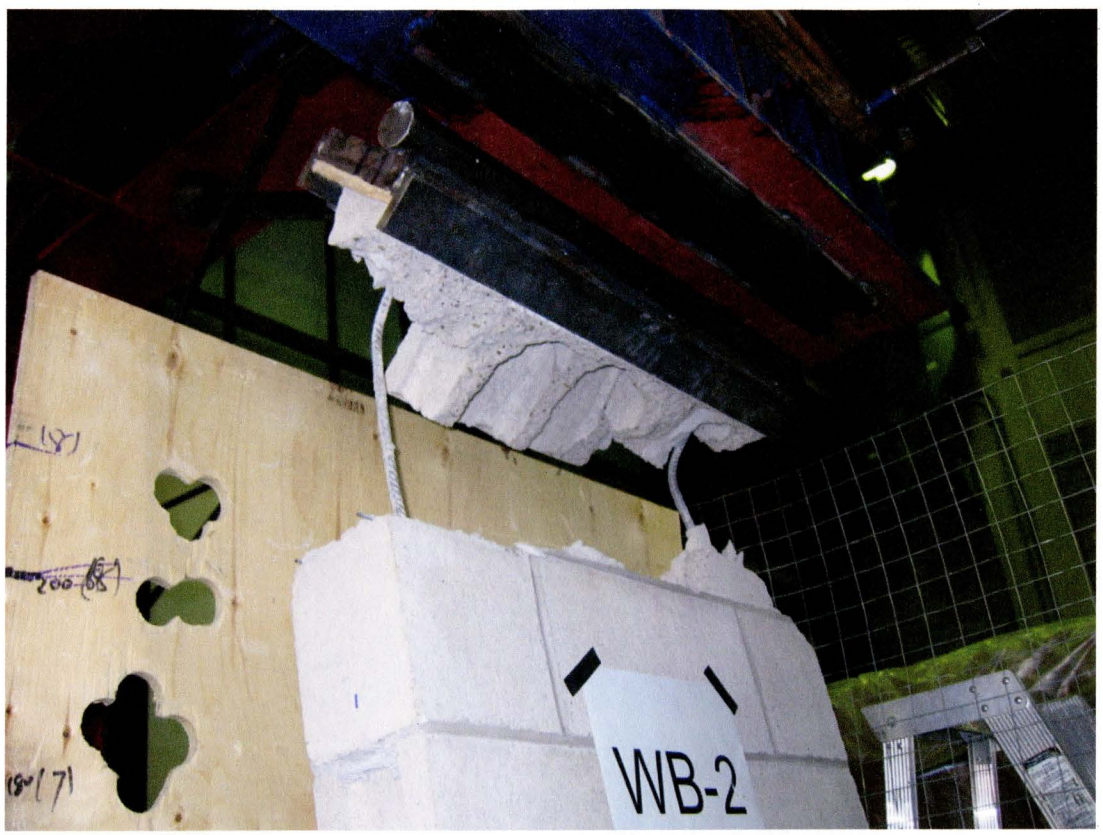

Figure 4.11 Failure mode of wall specimen WB-2

Figure 4.12 Failure mode of wall specimen WB-3

Vertical compressive load vs. lateral deflection curves for specimens in WB series are shown in Figure 4.13. As the eccentricity increases, the stiffness of the specimen at failure decreases which resulted in an increased lateral deflection and ductility. Referring to Figures 4.7 and 4.13, the ductility at failure for specimens in WB series indicated by a maximum ultimate deflection of less that 3 mm is less than that of specimens in WA series with a maximum ultimate lateral deflection of about 7 mm.

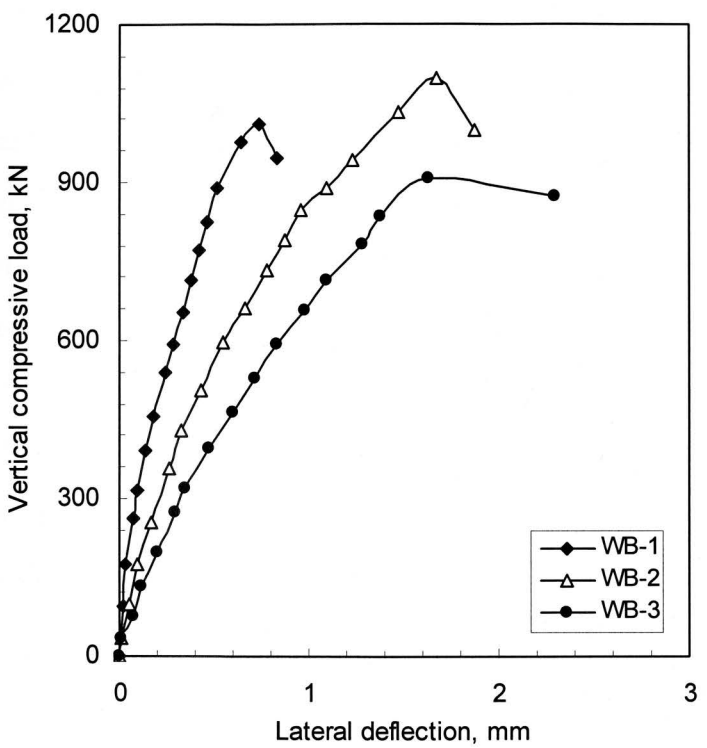

Figure 4.13 Vertical compressive load vs. lateral deflection curves for wall specimens in WB series

4.2.3 WC series (reverse curvature bending)

Three reinforced masonry wall specimens were tested in WC series under reverse curvature bending where the end loads were applied at the same magnitude of opposing

eccentricities. Specimens WC-1, WC-2, and WC-3 were tested with eccentricity magnitudes of $t/6$, $t/4$, and $t/3$, respectively.

The failure modes for specimens WC-1 and WC-2 are shown in Figure 4.14, and Figure 4.15, respectively. Both failure modes were predominantly compressive with specimen WC-1 showing more evident vertical splitting through the web at failure. It is noted that specimen WC-1 failed at the bottom portion of the specimen while the failure of specimen WC-2 occurred at the top portion. For equal reverse curvature bending, the wall specimen was essentially behaving as two simply supported half-height walls each under single curvature bending. The failure would therefore occur in either top or bottom portion of the specimen whichever is weaker. In the case of specimen WC-3, failure as shown in Figure 4.16 occurred in the bottom portion of the wall. The mortar joint at the second course opened up signifying tension cracking and rotation of the end. Crushing of masonry on the compressive face and spalling of the faceshell were observed as shown in Figure 4.17. In all cases, failure was explosive with no apparent warning. The failure concentrated in the end three courses, which is consistent with the location of maximum lateral deflection calculated using elastic analysis.

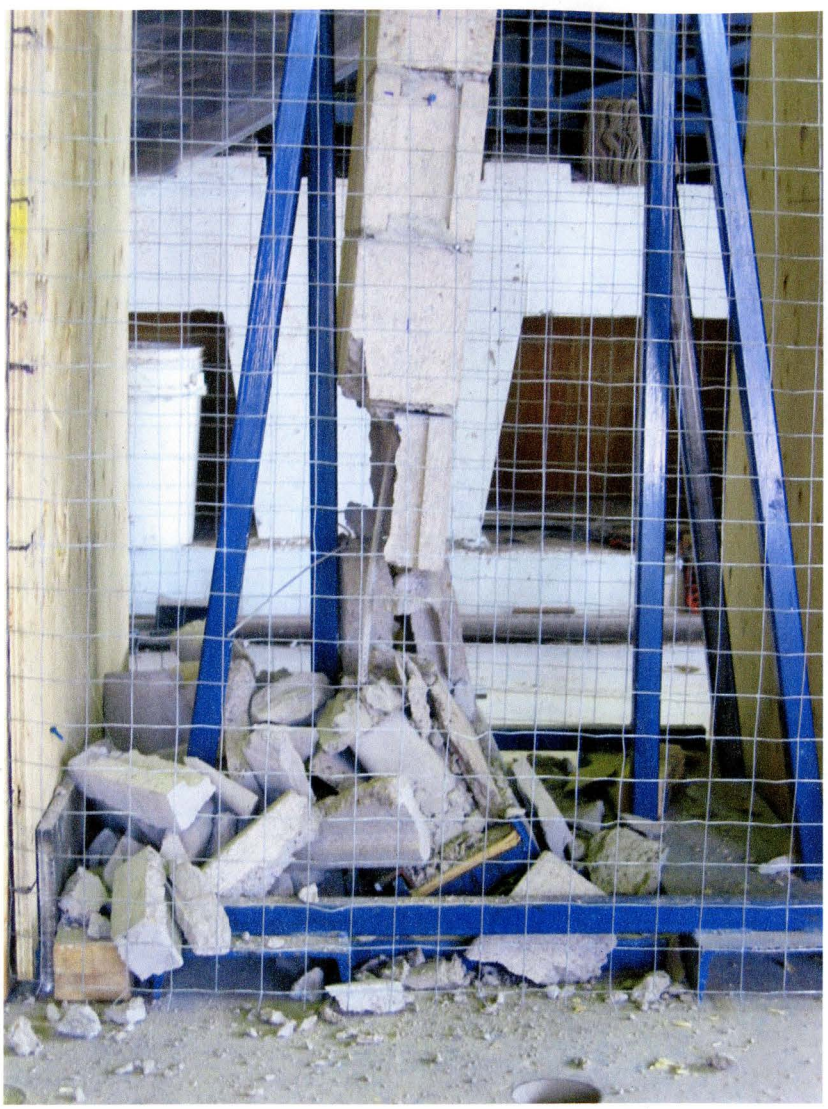

Figure 4.14 Failure mode of wall specimen WC-1

Figure 4.15 Failure mode of wall specimen WC-2

Figure 4.16 Failure mode of wall specimen WC-3

Figure 4.17 Crushing of compressive face in WC-3

Vertical compressive load vs. lateral deflection curves for WC series are shown in Figure 4.18. The deflection curve for specimen WC-1 remained almost linear up to the ultimate load. With an increase in eccentricity, nonlinear behavior became increasingly evident and occurred at earlier loading stage. The non-linearity was caused by a combination of material nonlinearity and geometrical nonlinearity. Compared with WA and WB series, WC series showed the least ductility at failure with the highest ultimate load.

Lateral deflections at seven locations along the height of wall WC-1 were monitored and recorded during the test. The deflected shape at various load levels based on the lateral deflections is shown in Figure 4.19. A reverse curvature characterized by inflection points was evident. Considering the random property and modular nature of masonry, the inflection point may not necessarily occur at mid-height of the member. In this case,

greater lateral deflections were recorded at the bottom portion of the specimen which caused the shift of the inflection point from being close to the mid-height to the top portion of the specimen.

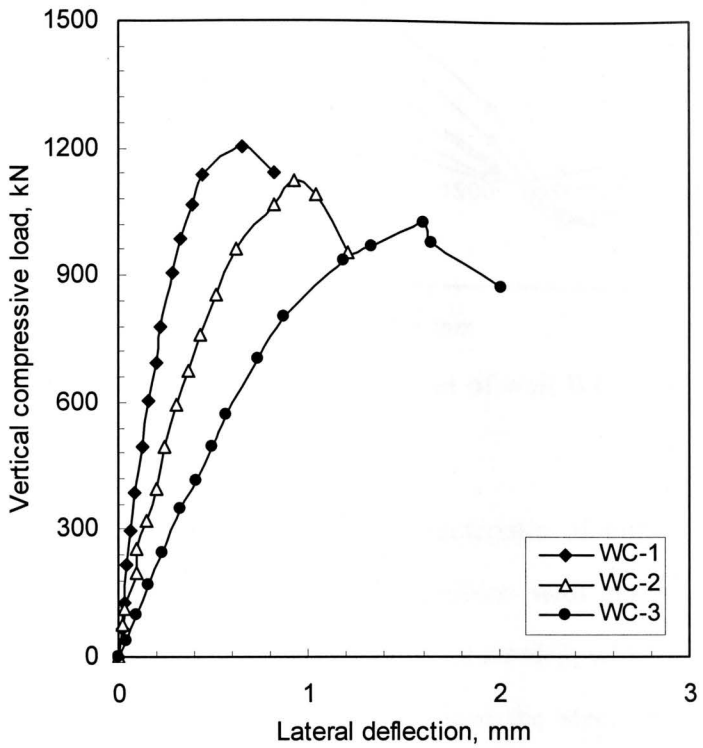

Figure 4.18 Vertical compressive load vs. lateral deflection curves for wall specimens in WC series

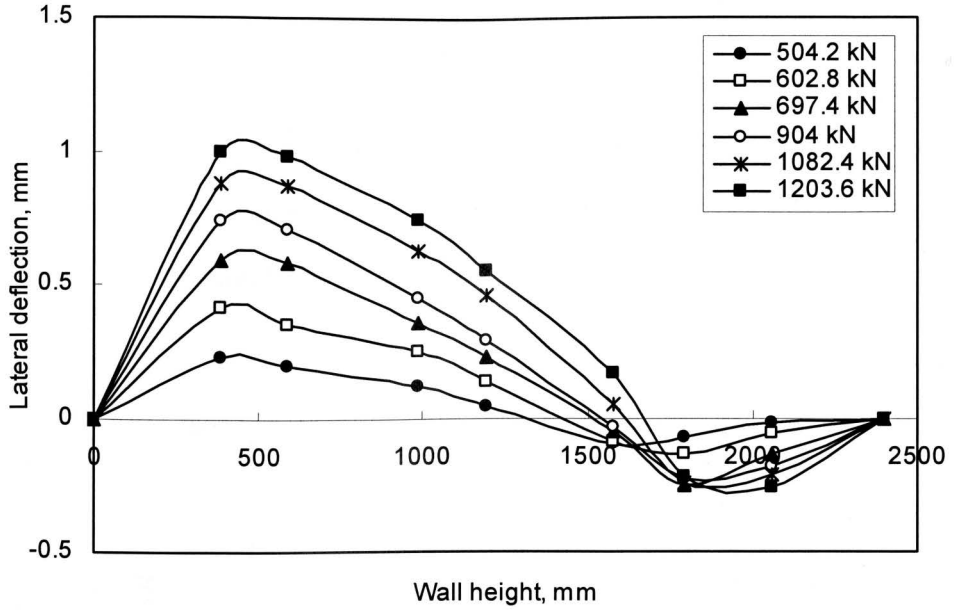

Figure 4.19 Deflection shapes of wall WC-1

The failures in the three series showed the characteristic of either pure compression failure or combined tension and compression failure with no pure tension failure observed. For walls tested at maximum eccentricity of e/t=1/3, while tensile cracking was observed, the crack depth was not sufficient to place the steel in tension or to cause yielding.

Figure 4.20 (a), (b) and (c) shows the compressive load plotted against lateral deflection curves are plotted for wall specimens tested with different e_1/e_2 ratios. It is evident that for wall specimens with a constant applied eccentricity, lateral deflections decrease and wall stiffness increase at failure as e_1/e_2 ratios change from 1.0 to 0.0, and then to -1.0. In Figure 4.20 (c) for walls tested at an eccentricity ratio of 1/3, the response of specimens WB-3 and WC-3 under asymmetrical single curvature and reverse curvature bending respectively, remained almost linear up to 90 per cent of the ultimate loads accompanied with a lateral deflection of less than 2 mm. Specimens WA-3 and WA-4 tested under symmetrical single curvature bending demonstrated evident non-linear behavior at about

70 per cent of the ultimate loads with a deflection of about 4 mm. It indicates that the wall specimens became stiffer which resulted in less deflection and higher capacity with e_1/e_2 ratio changing from 1.0 to 0.0 and to -1.0. This is corroborated by the observed failure modes where the failure of WC series walls was more sudden and explosive and showing more compression failure characteristics than that of WA series.

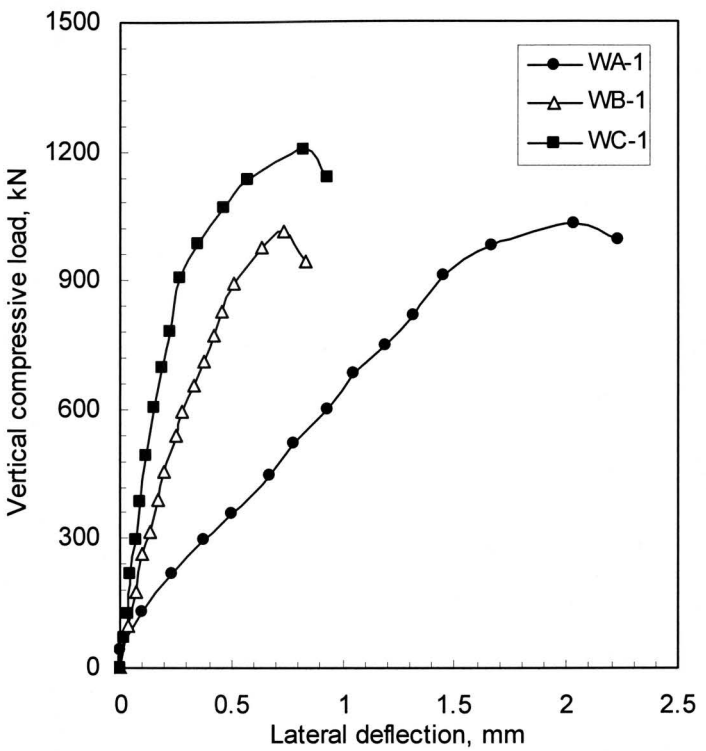

(a) Compressive load vs. lateral deflection curves for specimens with e/t =1/6

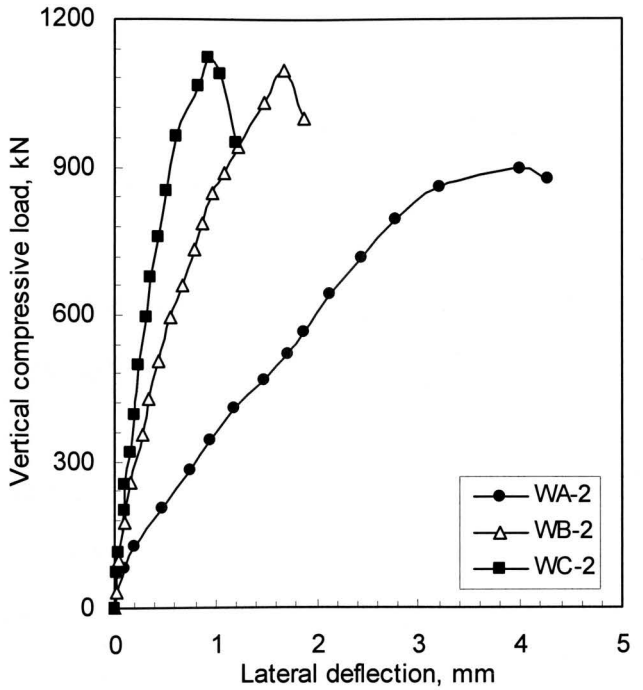

(b) Compressive load vs. lateral deflection curves for specimens with e/t =1/4

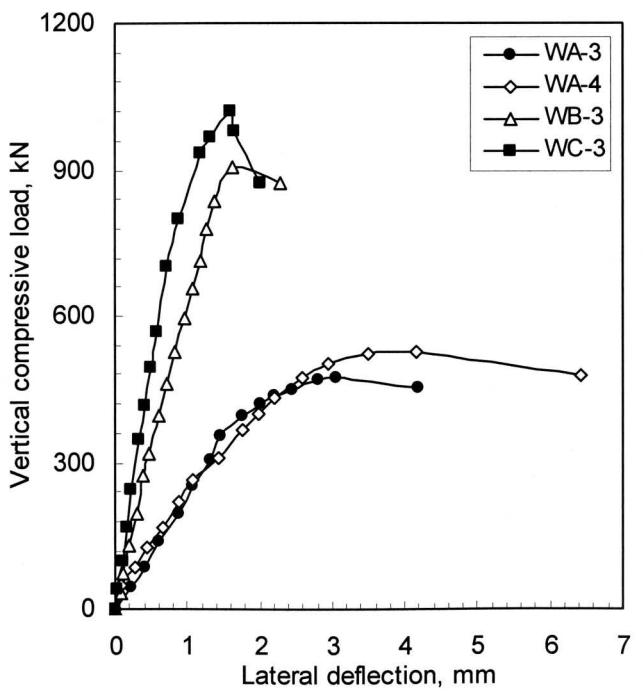

(c) Compressive load vs. lateral deflection curves for specimens with e/t =1/3

Figure 4.20 Comparison of load vs. lateral deflection curves for wall specimens with different e_1/e_2 ratios

4.3 Concluding Remarks

The experimental study involved the testing of ten large-scale partially grouted reinforced concrete masonry walls subjected to a number of combinations of vertical loads and end moment. Variables investigated included load eccentricity ratios (e/t) and end eccentricity ratios (e_1/e_2).

Test results showed that the capacities of walls tested in this program and their failure modes were a function of applied load eccentricities and the end moment conditions. In general, test data indicated a reduction in both load capacity and masonry wall stiffness with an increase of the eccentricity for all 3 tested series. The change of e_1/e_2 ratio from 1.0 to 0.0 to -1.0 led to increases of capacity and flexural rigidities of specimens.

Both compression failure and combined compression and tension failure were observed in three test series. The failure mode shifted from combined compression and tension failure characterized by the tensile cracking and masonry crushing to more pronounced compression failure characterized by masonry crushing and rebar buckling without evident tensile cracking as the eccentricity ratio, e/t, decreased for a constant e_1/e_2 ratio. A similar shift of failure mode was also observed as the e_1/e_2 ratio changed from 1.0 to 0.0 to -1.0 for specimens tested at a constant e/t ratio

CHAPTER V ANALYSIS AND COMPARISON OF TEST RESULTS

5.1 Introduction

Ultimate wall capacities and EI_{eff} values based on experimentally measured vertical deformation or deflected profile shape were compared with the values suggested in the current Canadian masonry design code (CSA S304.1-M04). Test results were also compared with values of experimental works by other researchers. Findings based on these comparisons and their implications to code design guidelines were presented and discussed in detail.

5.2 Comparison of Test Values and Code Values

For the design of masonry load-bearing walls including slenderness effect, the Canadian design code, CSA S304.1-M04, recommends that load and moment interaction be considered when calculating the cross-sectional strength and that the moment magnifier method be used to account for the slenderness effects. The strength interaction diagram for the masonry wall cross-section used in this research was determined using rectangular stress block theory in which a rectangular representation similar to the Whitney stress block in reinforced concrete is used to give a reasonable estimate of the magnitude and location of the resultant compressive force. A comparison of the *P-M* interaction diagram based on rectangular stress block theory and masonry wall capacities determined from the tests is presented in Figure 5.1. Experimentally determined material properties including masonry strength, f'_m, and steel yield strength, f_y, were used to calculate the *P-M* interaction diagram. It is noted that there are two experimental points associated with each specimen. The first point represents the applied moment, M_a, at the cross-section excluding slenderness effect, which is calculated as $P_u e$, while the second point represents the total moment, M_u, calculated as $P_u(e+ \Delta_u)$. The distance between

these two points represents the moment, M_s, caused by slenderness effect, which is defined as $P_u\Delta_u$. As seen in Figure 5.1, a comparison between the *P-M* interaction diagram and tested specimen capacities, excluding slenderness effect, shows in general, that the *P-M* interaction diagram based on rectangular stress block theory somewhat underestimates the wall capacities. This underestimation is more pronounced in the region of compression failure and is also more pronounced for WC and WB series than for WA series. For specimens WA-3 and WA-4 whose failure was largely initiated by tensile cracking, the *P-M* interaction diagram appears to provide a reasonable estimate of the cross-sectional strength. This observation is in line with the research work conducted by Liu (2002).

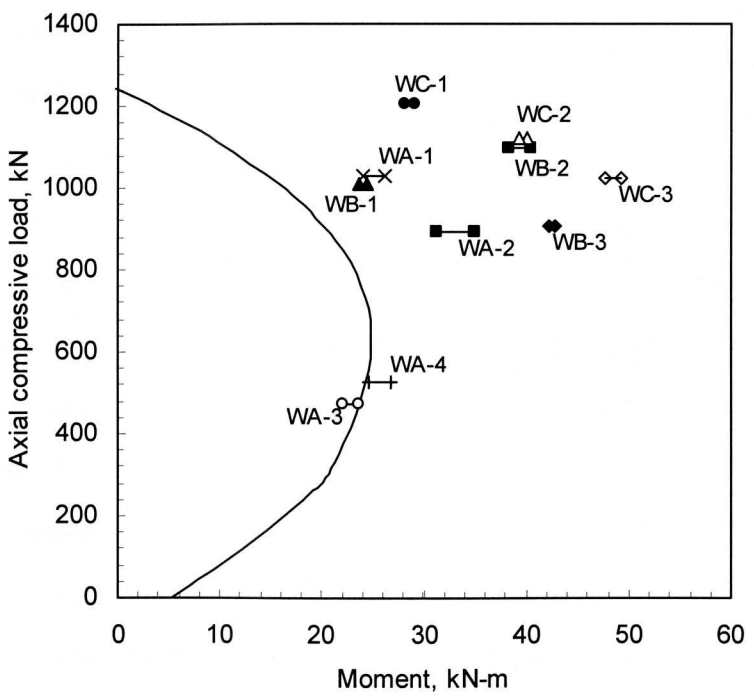

Figure 5.1 Comparison of *P-M* interaction diagram and test results

A comparison between the *P-M* interaction diagram and tested specimen capacities including slenderness effect shows a further enlarged discrepancy, which indicates that the secondary moment in slender compression members leads to decreased ultimate

capacity. The values of M_u, M_p, and M_s are listed Table 5.1 where M_p represents the primary moment without considering slenderness effect, M_s is the secondary moment caused by slenderness effect and M_u is the total applied moment at the cross-section. The ratio of M_s vs. M_u is also listed. In general, wall specimens in WA series have the largest portion of the total moment resulting from secondary moment, and specimens tested under reverse curvature bending have the least portion of their total moment coming from moment caused by slenderness effect. For example, more than 6 per cent to 10 per cent of the total moment in WA series resulted from the secondary moment. The percentage for wall specimens in WB series ranged from 3.4 per cent to 4.5 per cent, and up to 3.2 per cent in WC series was contributed by the secondary moment. This observation is consistent with the findings in the masonry wall compressive load vs. lateral deflection curves in which WA walls showed the largest lateral deflection while WC walls exhibited very small deflection at failure. However, no clear trend for the M_s/M_u values is shown within each series due to the limited wall specimens tested.

To evaluate the effectiveness of the moment magnifier method in the code to include the slenderness effect, slender masonry wall load-moment interaction diagram for the three series of wall specimens are plotted along with the experimental wall capacities (P_u, M_p) as shown in Figure 5.2. An iterative process was employed to determine the reduced *P-M* interaction curve based on moment magnifier method in CSA S304.1-M04. Points on the slender *P-M* interaction diagram represent the combined maximum primary moment and axial load a load-bearing member can resist. The discrepancy between test wall capacities with the load-moment interaction curves becomes much larger than that as shown in Figure 5.1, which indicates that secondary moment causes enlarged moment along masonry wall height and the masonry design code overly estimated the strength reduction due to slenderness effect.

Table 5.1 Values of M_u, M_p, M_s, and M_s/M_u

Specimen	Eccentricity e/t	End Moment Ratio e_1/e_2	M_u (kN-m)	M_p (kN-m)	M_s (kN-m)	M_s/M_u
WA-1	1/6, 1/6	1.0	26.1	24.0	2.1	0.081
WA-2	1/4, 1/4	1.0	34.9	31.3	3.6	0.103
WA-3	1/3, 1/3	1.0	23.6	22.1	1.5	0.064
WA-4	1/3, 1/3	1.0	26.8	24.6	2.2	0.082
WB-1	0, 1/6	0.0	24.4	23.6	0.8	0.033
WB-2	0, 1/4	0.0	40.2	38.4	1.8	0.045
WB-3	0, 1/3	0.0	43.8	42.3	1.5	0.034
WC-1	-1/6, 1/6	-1.0	28.9	28.1	0.8	0.027
WC-2	-1/4, 1/4	-1.0	40.5	39.3	1.2	0.029
WC-3	-1/3, 1/3	-1.0	49.4	47.7	1.7	0.032

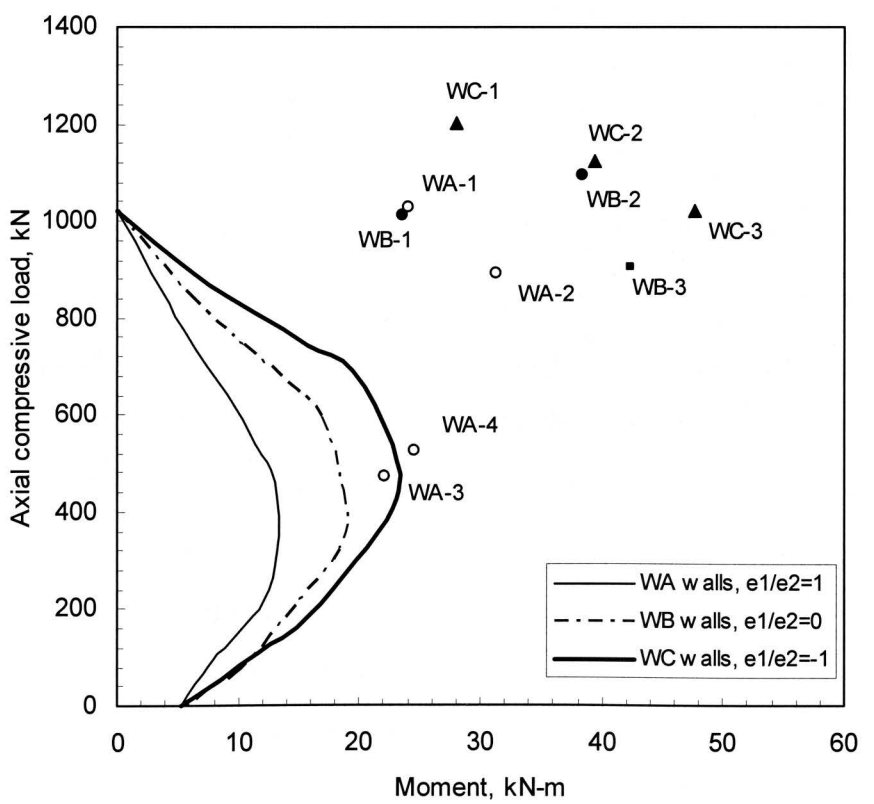

Figure 5.2 Comparison of slender *P-M* interaction diagram and test results

To evaluate the combined effectiveness of *P-M* interaction and moment magnifier method in the code, the masonry wall ultimate capacities predicted based on the cross-sectional strength were defined using *P-M* interaction relationship in combination with the slenderness effect calculated using moment magnifier method for the tested specimens were determined. Specimen WB-2 is taken as an example. The procedure for determining its predicted capacity is demonstrated schematically in Figure 5.3, in which the *P-M* interaction diagram was first determined based on the geometry of the specimen. An axial load vs. magnified moment curve based on moment magnifier method was then plotted. The intersection of the two curves is the corresponding predicted axial load, P_{theory}, and corresponding moment is M_{theory}. The experimental capacity of specimen WB-2 is also identified in the figure. The results of P_{theory} and M_{theory} for all the specimens are listed in Table 5.2 together with the experimentally determined masonry wall capacities.

The comparison in Table 5.2 shows that a large discrepancy exists between the code-based theoretical and experimental wall capacities. The coupled procedure including the evaluation of wall cross-sectional strength using stress-block method and secondary moment effect using moment magnifier method is shown to result in a conservative estimation for load-bearing reinforced concrete masonry wall capacities. An accurate estimation of cross-sectional capacity must consider the nonlinear masonry material property and strain gradient effect in which larger compressive stress at the extreme compressive fiber of the cross-section than masonry f'_m determined from prism test exits for walls under eccentric compressive loading (Drysdale et al (1999)). The investigation on the strain gradient effect is being conducted in an independent research by another graduate student. The inherent correctness of moment magnifier method with an emphasis on the evaluation of masonry wall effective flexural rigidity is discussed in the following sections.

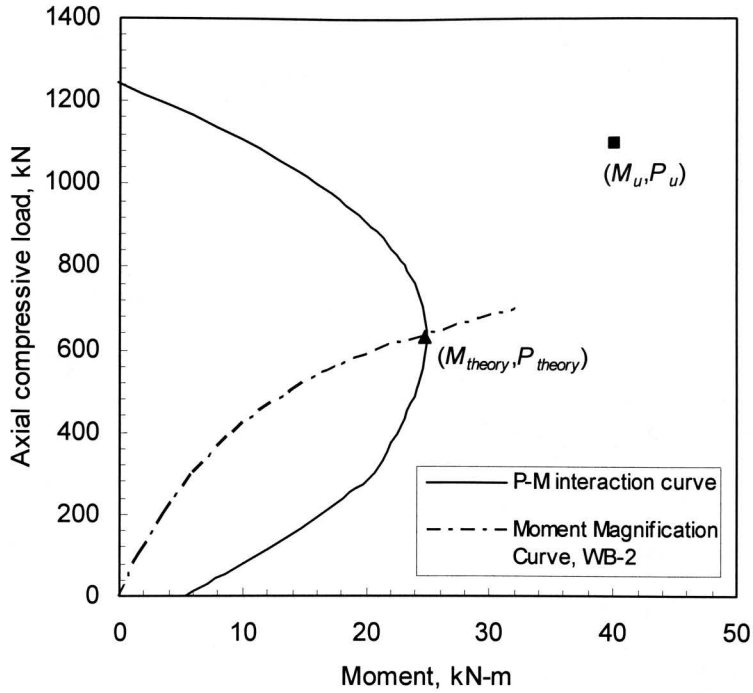

Figure 5.3 Determination of theoretical wall capacity

Table 5.2 Experimental and theoretical wall capacities

Specimen	Eccentricity e/t	e_1/e_2	P_u (kN)	P_{theory}	M_u	M_{theory}
WA-1	1/6, 1/6	1.0	1029.3	507	26.1	23.7
WA-2	1/4, 1/4	1.0	894.9	372	34.9	21.8
WA-3	1/3, 1/3	1.0	474.3	285	23.6	20.3
WA-4	1/3, 1/3	1.0	526.8	285	26.8	20.3
WB-1	0, 1/6	0.0	1011.7	724	24.4	23.8
WB-2	0, 1/4	0.0	1096.8	612	40.2	24.3
WB-3	0, 1/3	0.0	906.5	478	43.8	23.4
WC-1	-1/6, 1/6	-1.0	1203.6	637	28.9	24.2
WC-2	-1/4, 1/4	-1.0	1124.2	517	40.5	23.6
WC-3	-1/3, 1/3	-1.0	1022.2	400	49.4	22.5

5.3 Effective Flexural Rigidity of Concrete Masonry Walls

5.3.1 General

Moment versus curvature curves for the wall specimens were established based on the measurements during each test, and used to determine effective flexural rigidity, EI_{eff}, for walls under various loading combinations at the time of failure. EI_{eff} values from this experimental program, together with proposed EI_{eff} values from reported available literature are then compared with values suggested by the Canadian masonry design code, CSA S304.1-M04. Variables involved in the comparison are axial load eccentricity ratio (e/t), slenderness ratio (h/t), and end moment ratio (e_1/e_2).

5.3.2 Moment versus curvature relationship and flexural rigidity of masonry

Moment versus curvature curves were plotted and used to determine EI_{eff} at failure for the wall specimens based on Equation (5.1).

$$EI = \frac{M}{\varphi} \tag{5.1}$$

In this relationship, M is the calculated moment including the secondary moment due to lateral deflection and φ is the measured curvature of the section where M is calculated. M can be expressed as $P(e+\Delta)$, where P is the compressive load applied at the two ends of the walls, e is the eccentricity of the applied load, Δ is the measured lateral deflection at the cross-section where predicted maximum deflection occurs. A typical moment vs. curvature relationship and the definition of EI_{eff} are shown in Figure 5.4.

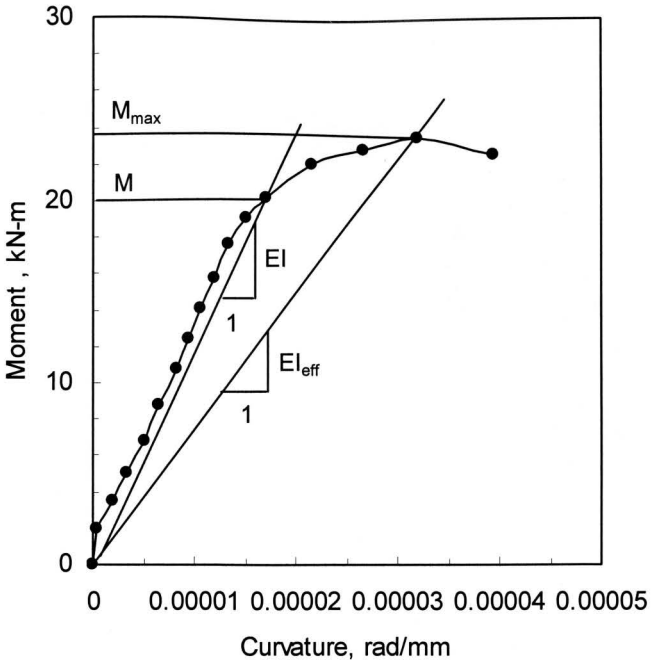

Figure 5.4 Illustration of determining effective flexural rigidity

Since two different instrumentation schemes were used in this experimental program, two methods were used in the calculation of φ. For specimens WA-1 and WC-1, a deflected shape was determined based on the lateral deflections measured at seven locations along the height of the wall. Using the curve-fitting technique in Matlab 7.0.1, an 8^{th} order polynomial expression was used to approximate the deflection curves obtained at ultimate as shown in Figure 5.5 (a) and (b) for specimens WA-1 and WC-1, respectively. C urve-fitting was performed with reliable accuracy with the least curve-fitting correlation coefficient R^2 larger than 0.96. The curvature, φ, at various cross-sections along the height of the wall can then be calculated by differentiating the shape expression twice.

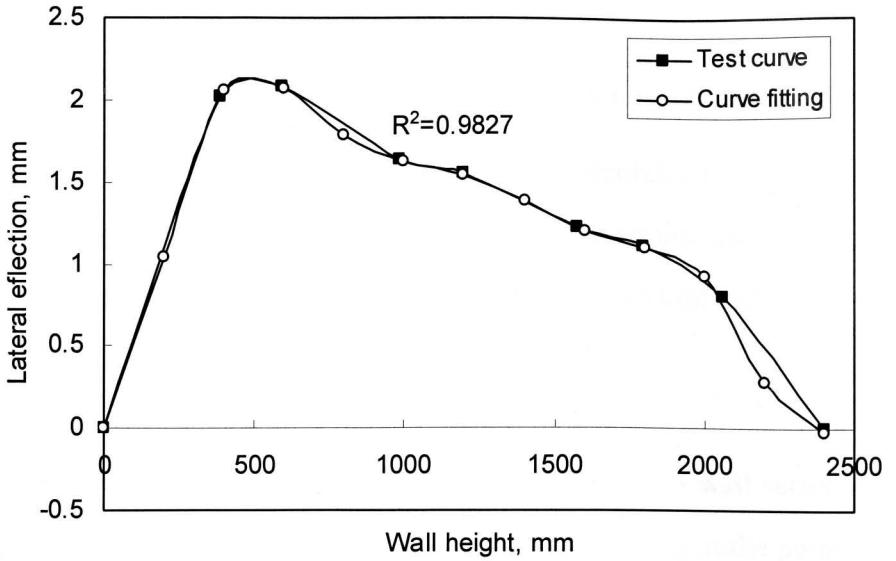

(a) Wall specimen WA-1

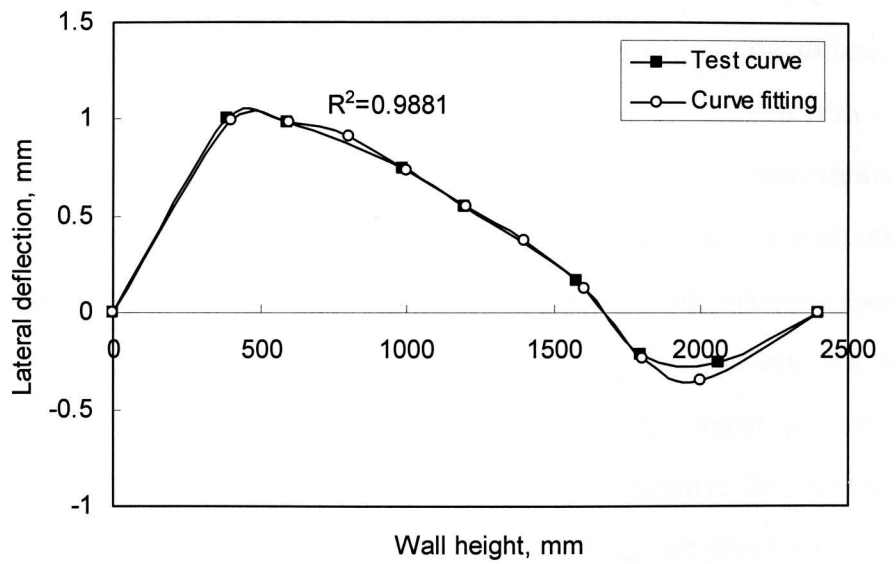

(b) Wall specimen WC-1

Figure 5.5 Curve-fitting for WA-1 and WC-1

For the remaining specimens, the curvature φ was determined using vertical deformations measured on both tensile and compressive faces of the wall based on Equation (5.2):

$$\varphi = \frac{\varepsilon_1 - \varepsilon_2}{t} \tag{5.2}$$

where t is the wall thickness, ε_1 and ε_2 are the strains on the compression and tension faces of the wall specimens. These strains are calculated by dividing the vertical deformations by gauge lengths. In this research, surface strains and lateral deflections used in the calculation of curvature were measured at the sections where the moment is predicted to be maximum and thus EI_{eff} to be minimum.

Experimentally obtained moment vs. curvature curves for all 3 wall series are presented in Figure 5.6 to 5.8 and values of effective flexural rigidity EI_{eff} at the point of maximum moment and axial load combinations are listed in Table 5.3. As can be seen in Figures 5.6 to 5.8, similar trend is evident for specimens in all 3 series. On average, moment vs. curvature curves remained almost linear up to about 70 per cent of the ultimate moment capacity. Apparent non-linearity is shown after that point accompanied with a reduction in flexural rigidity as the curvature increases. Consistent with observations made in compressive load vs. lateral deflection responses, this non-linearity is attributed to both material nonlinearity resulting from increased stress levels in the masonry specimen and geometric nonlinearity caused by the compounding secondary effect. For a constant value of end eccentricity ratio e_1/e_2, specimens tested with larger e/t ratios showed greater curvature values at failure which indicated a lower effective flexural rigidity, EI_{eff}, for these specimens. In Table 5.3 experimental values of EI_{eff} are presented in normalized form obtained by dividing each value by EI_0, the initial flexural rigidity of the uncracked cross-section.

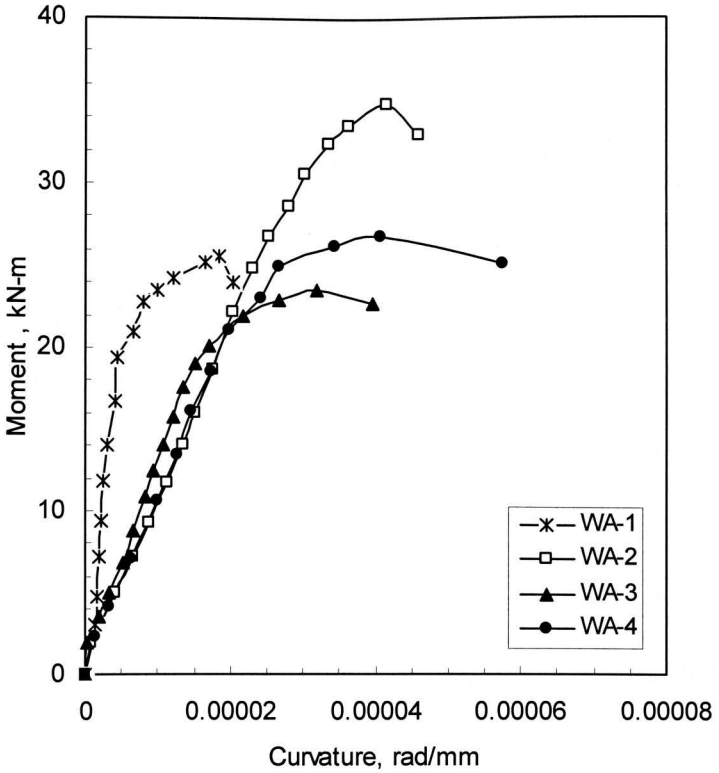

Figure 5.6 Moment vs. curvature curves for wall specimens with e_1/e_2=1.0

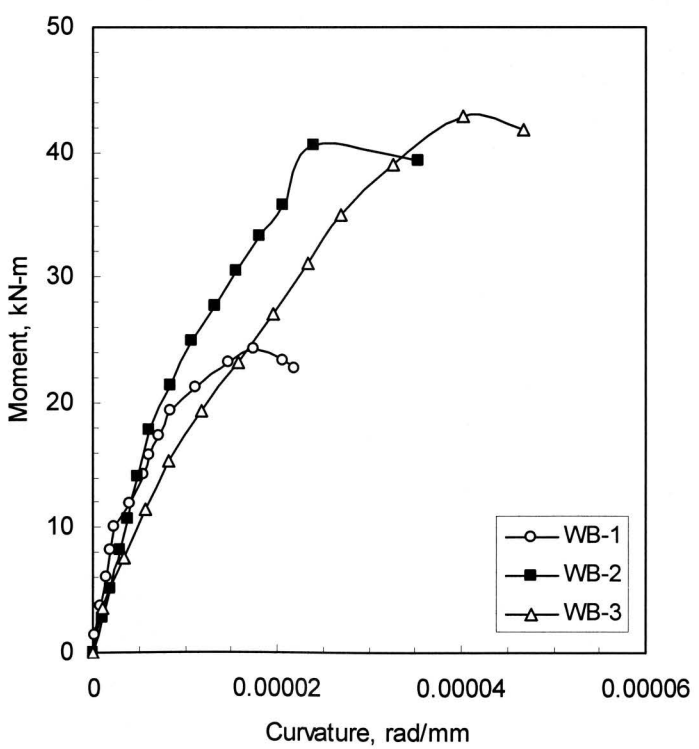

Figure 5.7 Moment vs. curvature curves for wall specimens with e_1/e_2=0.0

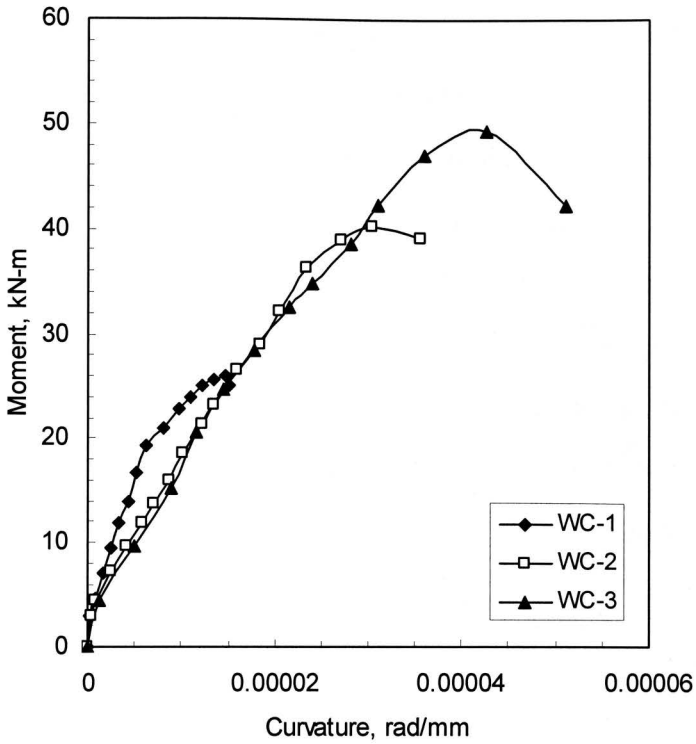

Figure 5.8 Moment vs. curvature curves for wall specimens with e_1/e_2=-1.0

Table 5.3 Experimental results of flexural rigidities at failure

Specimen	Eccentricity e/t	End Moment Ratio e_1/e_2	Ultimate Moment M_u (kN-m)	EI_{eff}/EI_0
WA-1	1/6, 1/6	1.0	26.1	0.638
WA-2	1/4, 1/4	1.0	34.9	0.360
WA-3	1/3, 1/3	1.0	23.6	0.315
WA-4	1/3, 1/3	1.0	26.8	0.292
WB-1	0, 1/6	0.0	24.4	N/A
WB-2	0, 1/4	0.0	40.2	0.403
WB-3	0, 1/3	0.0	43.8	0.352
WC-1	-1/6, 1/6	-1.0	28.9	0.819
WC-2	-1/4, 1/4	-1.0	40.5	0.600
WC-3	-1/3, 1/3	-1.0	49.4	0.413

Due to a premature failure of specimen WB-1, the test results were not included in the calculation. It can be seen that for all three series, effective flexural rigidities of masonry specimens prior to failure decrease with an increase in the applied load eccentricities. For example, for specimen WA-3 tested at an e/t of 1/3, its mid-height cross-section maintained about 34 per cent of initial flexural rigidity at failure while specimen WA-1 tested at an e/t of 1/6, about 65 per cent of initial flexural rigidity existed in the mid-height cross-section at ultimate. Similar observations can be made for specimens tested in WB and WC series. The variation of effective flexural rigidities for wall specimens WA-3 and WA-4 is approximately 8%, which indicates the test results obtained are reliable if recall the small variation of ultimate load capacity for these two specimens. The relationship of EI_{eff} with e/t and e_1/e_2 is further illustrated in Figure 5.9, in which the normalized flexural rigidity values were plotted against the axial load eccentricity ratio.

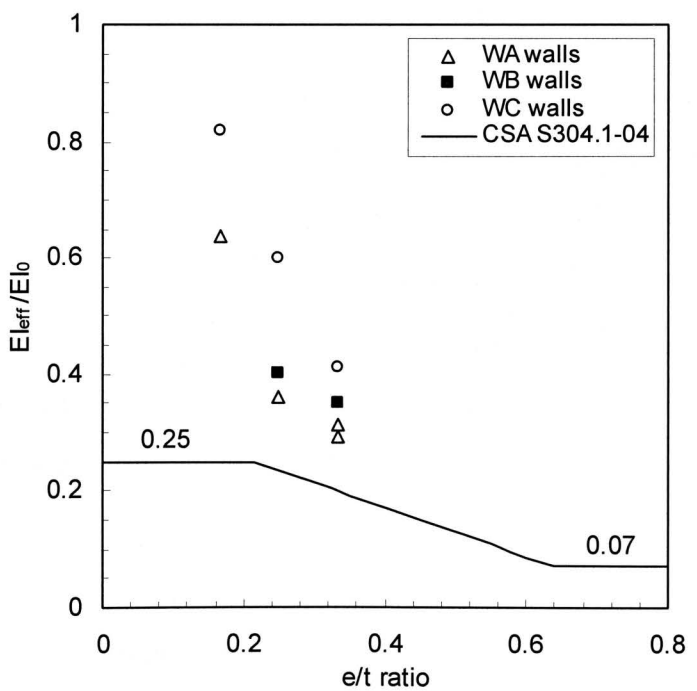

Figure 5.9 EI_{eff}/EI_0 vs. e/t for wall specimens and code values

The value of e is the applied load eccentricity and does not include lateral mid-height deflection of walls, and t is the masonry wall thickness. For comparison, a curve determined using the code equations (Equation (2.24)) is also included in the figure where 0.25 represents the upper limit and 0.07 represents the lower limit of EI_{eff} values. As eccentricity ratio increases, all three curves representing specimens in the three series showed a decrease in EI_{eff} values. The variation of EI_{eff} values is due to the nonlinear stress-strain relationship for masonry in compression and the reduction of the moment of inertia caused by cracking of the cross-section. Under different loading conditions, the significant difference in EI_{eff} is attributed to the interaction between these two factors. The load vs. lateral deflection curves presented in Chapter IV indicate that, for constant values of slenderness and end eccentricity ratio, large deflections and low ultimate capacity occur for high applied eccentricity while small deflections and high ultimate capacity correspond to low applied eccentricity. When the axial load is high, the failure of the specimen is largely under compression with small lateral deflections and little tensile cracking. The reduction of EI_{eff} is mainly caused by the nonlinearity of the stress-strain relationship. While for specimens failed by tension or combined tension and compression where tensile cracking is developed to certain degree to the thickness of the wall cross-section, the reduction of EI_{eff} is primarily the result of a reduced cross-sectional area caused by tensile cracking. Although the material non-linearity and the extent of tensile cracking are concurrent and dependent on each other, it appears that the reduction of EI_{eff} is more significant as a result of the reduced cross-section caused by tensile cracking rather than as a result of material non-linearity for parameters investigated herein.

The effect of various e_1/e_2 ratios on masonry wall flexural rigidity is also demonstrated in Figure 5.9. For a given value of e/t, EI_{eff} increases as e_1/e_2 changes from 1.0 to 0.0 and then to -1.0. For e_1/e_2 ratios equal to 0.0 and –1.0, the maximum primary moment, Pe,

occurs at one end of the specimen, which does not coincide with the location of the maximum lateral deflection. The maximum lateral deflection occurs somewhere between the mid-height and ends rather than at the mid-height of the specimen as in the case of e_1/e_2=1.0. It is expected and confirmed from the tests that the lateral deflection for former cases are smaller due to the confinement by the ends, which resulted in less tensile cracking prior to failure. The failure of specimens tested at e_1/e_2 equal to 0.0 and –1.0 was increasingly sudden and predominated by compression failure with a large portion of wall specimen located away from the failed cross-section remaining intact, which contributed to higher EI_{eff} values. In the case of e_1/e_2=1.0, the location of maximum lateral deflection and maximum primary moment coincide, which leads to a greater secondary moment resulting in significant tensile cracking on the tension surface of the specimen. The failure of such specimens is predominantly tension controlled. A specific example is given by the change of failure modes from tension controlled failure of specimen WA-3, for example, to the combined tension and compression failure mode of specimen WC-3 which had higher flexural rigidities prior to failure.

A comparison of experimental EI_{eff} values with the code curve in Figure 5.9 shows that while CSA S304.1-04 agrees with the general variation trend of EI_{eff} with the increase of e/t ratios, it underestimates EI_{eff} values at impending failure especially for walls failed in a compression failure mode. This underestimation is more pronounced for walls bent in asymmetrical single curvature and reverse curvature. This underestimation leads to conservative estimation and a variable factor of safety for ultimate moment capacity.

5.3.3 Design implications

Design implications of using code EI_{eff} values and the experimental EI_{eff} values obtained in this research are discussed in this section.

To evaluate the effectiveness of the moment magnifier method in the code to include the slenderness effect, axial capacities of the ten specimens were predicted using code equations and compared with the capacities measured experimentally. In the procedure, the effective flexural rigidity was determined first using code Equation (2.24) and the predicted load, P_{pred}, was then back-calculated using the moment magnifier method with experimental total moment values as the magnified moment. The predicted axial load capacity represents the axial load that can be applied on a wall to cause magnified moments which are equal to the actual total moments the wall sustained in the test. A comparison of tested axial capacity, P_u and calculated P_{pred} is illustrated in Figure 5.10. Each vertical line represents a single specimen, with the upper point on the line representing the tested wall capacity, and the lower point representing the calculated P_{pred} associated with experimental total moment values. In all cases, the code predicted axial load capacities, P_{pred}, are lower than the actual experimental axial load capacities. This observation indicates that moment magnifier method over estimates the detrimental effect of slenderness on masonry wall strength. However, the wall in reality can take additional load beyond this axial load level. The ratios of experimental axial load, P_u, to the back-calculated axial load, P_{pred}, are listed in Table 5.4 with the largest value equal to 1.88 for specimen WA-1.

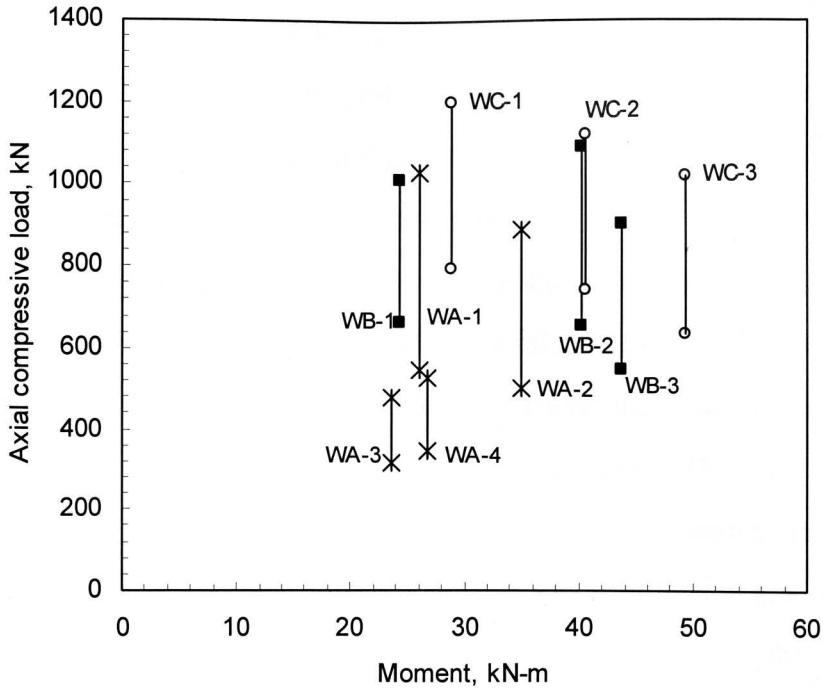

Figure 5.10 Experimental results and wall capacities based on moment magnifier method

Table 5.4 Comparison between experimental P_u and predicted P_{pred}

Specimen	P_u (kN)	M_u (kN-m)	P_{pred} (kN)	P_u/P_{pred}
WA-1	1029.3	26.1	547.6	1.88
WA-2	894.9	34.9	501.3	1.79
WA-3	474.3	23.6	316.4	1.50
WA-4	526.8	26.8	342.0	1.54
WB-1	1011.7	24.4	664.0	1.52
WB-2	1096.8	40.2	660.4	1.66
WB-3	906.5	43.8	548.8	1.65
WC-1	1203.6	28.9	796.7	1.51
WC-2	1124.2	40.5	747.6	1.50
WC-3	1022.2	49.4	640.8	1.60

A new moment magnifier curve determined based on experimental EI_{eff} value for the same specimens as the old moment magnifier curve determined based on code EI_{eff} value is added in Figure 5.3 and illustrated in Figure 5.11. The new curve approaches the point of experimental wall capacity on the curve much closer than the old curve, which indicates that moment magnifier method based on the experimental EI_{eff} values gives good estimation for load-bearing wall slenderness effect. However, it is also observed that the intersection of the new moment magnifier curve and *P-M* interaction diagram still underestimates the actual masonry wall capacity. This is due to the overly-conservative nature of *P-M* interaction for estimating masonry wall cross-sectional strength. Masonry material nonlinearity and strain gradient effect in which larger compressive stress at the extreme compressive fiber of the cross section than masonry uniaxial compressive strength, f'_m, will increase the moment capacity of masonry walls, which are needed in an accurate estimation of cross-sectional capacity.

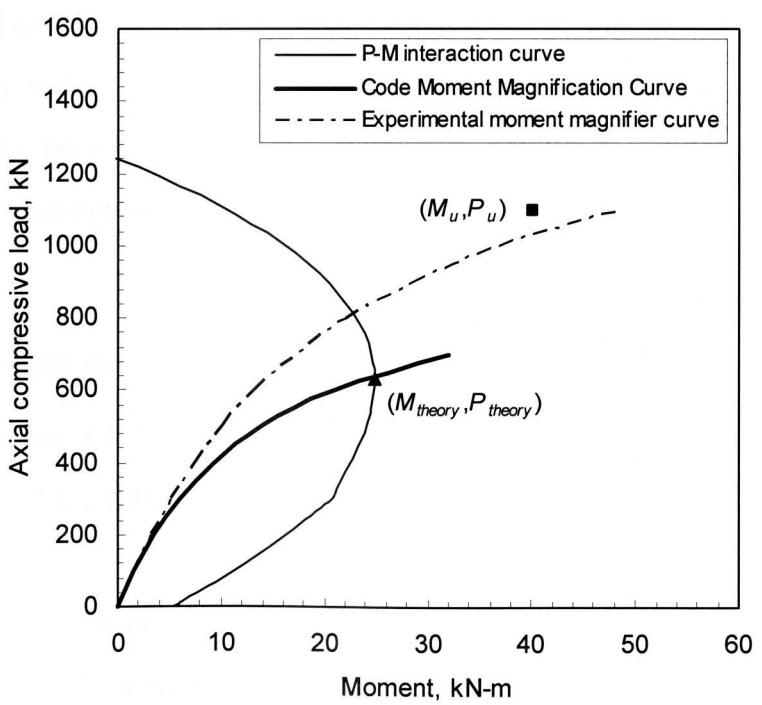

Figure 5.11 Moment magnifier curves determined from code and experimental EI_{eff} values

5.3.4 Experimental EI_{eff} values, Canadian code EI_{eff} values, and proposed EI_{eff} equations

It is recognized that the experimental data obtained in this research is limited and thus insufficient to be conclusive with regard to the validity of the code *EI* equations. Therefore, a total of 92 EI_{eff} values from the masonry wall tests conducted by Hatzinikolas et al. (1978), Aridru (1997), and Liu (2002) were obtained, including 75 EI_{eff} values for reinforced walls and 17 for plain masonry walls with various geometric and loading characteristics. All the flexural rigidity values, plus nine EI_{eff} values for reinforced concrete masonry walls determined in the current experimental program are compared with the recommended EI_{eff} values in the current Canadian masonry design code, CSA S304.1-M04 to investigate its inherent correctness in masonry load-bearing wall design. Some of the proposed equations from the previous research are also evaluated for their accuracy of estimating the effective flexural rigidity of eccentrically loaded masonry walls. The effects of compressive load eccentricity, slenderness ratio, and end moment ratio on the effective flexural rigidity of load-bearing walls prior to failure are also investigated.

5.3.4.1 Experimental flexural rigidity values from available literature

Tables 5.5, 5.6 and 5.7 list the EI_{eff} values obtained from Hatzinikolas et al. (1978), Aridru (1997), and Liu (2002), respectively.

In the masonry wall test program conducted by Hatzinikolas et al. (1978), both plain and reinforced masonry block walls of 1000mm long with two different slenderness ratios of 13.8 and 18.0 were tested. Three different reinforcement patterns including three 3M bars, three 6M bars and three 9M bars were used. Wall specimens were loaded eccentrically

causing symmetrical and non-symmetrical single curvature bending. Various end eccentricity ratios applied on the wall specimens as well as the experimental EI_{eff} values are listed in Table 5.5 for both reinforced and plain masonry walls.

The experimental program conducted by Aridru (1997) was designed to investigate the behavior of concrete masonry walls bent in symmetrical single curvature under eccentric compressive loading. Wall specimens were 1200mm high by 800mm long with different reinforcing patterns and grouting patterns where reinforcing patterns included both singly-reinforcing and doubly-reinforcing while grouting patterns included partially grouted and fully grouted walls. Eccentricity ratios applied on both ends of the wall specimens were 0.18, 0.27, and 0.36. EI_{eff} values obtained in this research are listed in Table 5.6 for both reinforced and plain masonry walls.

Table 5.5 EI_{eff} values from Hatzinikolas et al. (1978)

t (mm)	Rebar	h/t	e/t	e_1/e_2	EI_{eff}/EI_0
194	3-9M	13.8	0.17	1.0	0.73
	3-9M	13.8	0.33	1.0	0.60
	3-9M	13.8	0.39	1.0	0.53
	3-9M	13.8	0.46	1.0	0.11
194	3-6M	18.0	0.17	1.0	0.83
	3-6M	18.0	0.33	1.0	0.44
	3-6M	18.0	0.39	1.0	0.22
	3-6M	18.0	0.46	1.0	0.14
194	3-3M	18.0	0.17	-1.0	0.71
	3-3M	18.0	0.33	-1.0	0.18
	3-3M	18.0	0.39	-1.0	0.05
194	0	13.8	0.17	1.0	0.75
	0	13.8	0.33	1.0	0.50
	0	13.8	0.39	1.0	0.48
194	0	18.0	0.17	0.0	0.67
	0	18.0	0.33	0.0	0.46
	0	18.0	0.39	0.0	0.32
	0	18.0	0.46	0.0	0.23

Table 5.6 EI_{eff} values from Aridru (1997)

t (mm)	Rebar	h/t	e/t	e_1/e_2	EI_{eff}/EI_0
140	2-10M	8.5	0.18	1.0	0.79
	2-10M	8.5	0.18	1.0	0.72
	2-10M	8.5	0.18	1.0	0.75
	2-10M	8.5	0.18	1.0	0.72
	2-10M	8.5	0.18	1.0	0.73
140	2-10M	8.5	0.27	1.0	0.38
	2-10M	8.5	0.27	1.0	0.50
	2-10M	8.5	0.27	1.0	0.35
	2-10M	8.5	0.27	1.0	0.36
	2-10M	8.5	0.27	1.0	0.52
	2-10M	8.5	0.27	1.0	0.48
140	2-10M	8.5	0.36	1.0	0.32
	2-10M	8.5	0.36	1.0	0.33
	2-10M	8.5	0.36	1.0	0.34
	2-10M	8.5	0.36	1.0	0.30
	2-10M	8.5	0.36	1.0	0.33
	2-10M	8.5	0.36	1.0	0.39
	2-10M	8.5	0.36	1.0	0.22
	2-10M	8.5	0.36	1.0	0.20
	2-10M	8.5	0.36	1.0	0.22

a) Singly-reinforced wall specimens

Table 5.6 EI_{eff} values from Aridru (1997)-(cont'd)

t (mm)	Rebar	h/t	e/t	e_1/e_2	EI_{eff}/EI_0
140	4-10M	8.5	0.27	1.0	0.39
	4-10M	8.5	0.27	1.0	0.31
	4-10M	8.5	0.27	1.0	0.48
	4-10M	8.5	0.27	1.0	0.30
	4-10M	8.5	0.27	1.0	0.33
	4-10M	8.5	0.27	1.0	0.35
	4-10M	8.5	0.27	1.0	0.37
	4-10M	8.5	0.27	1.0	0.34
140	4-10M	8.5	0.36	1.0	0.20
	4-10M	8.5	0.36	1.0	0.24
	4-10M	8.5	0.36	1.0	0.24
	4-10M	8.5	0.36	1.0	0.23
	4-10M	8.5	0.36	1.0	0.23
	4-10M	8.5	0.36	1.0	0.20
	4-10M	8.5	0.36	1.0	0.22
	4-10M	8.5	0.36	1.0	0.22

(b) Doubly-reinforced wall specimens

Table 5.6 EI_{eff} values from Aridru (1997)-(cont'd)

t (mm)	Rebar	h/t	e/t	e_1/e_2	EI_{eff}/EI_0
140	0	8.5	0.18	1.0	0.75
	0	8.5	0.18	1.0	0.80
	0	8.5	0.18	1.0	0.84
	0	8.5	0.18	1.0	0.91
	0	8.5	0.18	1.0	0.75
140	0	8.5	0.36	1.0	0.45
	0	8.5	0.36	1.0	0.43
	0	8.5	0.36	1.0	0.64
	0	8.5	0.36	1.0	0.65
	0	8.5	0.36	1.0	0.60

(c) Plain wall specimens

Liu (2002) tested thirty-six reinforced specimens including both singly and doubly reinforced walls with pinned support conditions under pure axial loading and combined axial and lateral loading. Flexural rigidities, EI_{eff}, at the time of failure for walls under combined axial and lateral loading are shown in Table 5.7.

Table 5.7 EI_{eff} values from Liu (2002)

t (mm)	Rebar	h/t	e/t	e_1/e_2	EI_{eff}/EI_0
140	2-10M	8.5	0.58	1.0	0.067
	2-10M	8.5	0.72	1.0	0.071
	2-10M	8.5	0.74	1.0	0.077
	2-10M	8.5	0.57	1.0	0.159
	2-10M	8.5	0.53	1.0	0.165
	2-10M	8.5	0.54	1.0	0.151
	2-10M	8.5	0.46	1.0	0.215
	2-10M	8.5	0.42	1.0	0.207
	2-10M	8.5	0.46	1.0	0.186
	2-10M	8.5	0.4	1.0	0.347
	2-10M	8.5	0.42	1.0	0.295
	2-10M	8.5	0.37	1.0	0.381
	2-10M	8.5	0.27	1.0	0.670
	2-10M	8.5	0.26	1.0	0.580
	2-10M	8.5	0.2	1.0	0.830
140	4-10M	8.5	0.98	1.0	0.188
	4-10M	8.5	0.9	1.0	0.105
	4-10M	8.5	0.95	1.0	0.117
	4-10M	8.5	0.67	1.0	0.185
	4-10M	8.5	0.6	1.0	0.169
	4-10M	8.5	0.45	1.0	0.225
	4-10M	8.5	0.43	1.0	0.240
	4-10M	8.5	0.35	1.0	0.487
	4-10M	8.5	0.36	1.0	0.368
	4-10M	8.5	0.27	1.0	0.678
	4-10M	8.5	0.26	1.0	0.682
	4-10M	8.5	0.22	1.0	0.835
	4-10M	8.5	0.23	1.0	0.759

All EI_{eff}/EI_0 values listed in above tables together with the experimentally determined EI_{eff}/EI_0 values in this research are plotted in Figure 5.12 against the compressive load eccentricity ratios. In the figure, flexural rigidity values for plain masonry and reinforced masonry walls are identified. The design curves for both plain and reinforced masonry walls based on the code equations are also included with upper and lower limits indicated. It is found that for all test programs with those described wall cross-sectional configurations, only minor variation exists in the EI_{eff}/EI_0 values determined using code equations. Therefore, for simplification, one representative code EI_{eff} curve based on the specimen cross-sectional properties in this research was plotted for reinforced walls with the same upper and lower limits as determined previously. The trend of presented data confirms the observation made in this research that the increase of eccentricity ratios results in a reduction in EI_{eff} values. Comparing with the code curves, it can be seen that only 4 out of 84 of the reinforced EI_{eff} points lie below the code curve, which clearly indicates the conservatism of the flexural rigidity values given by the Canadian masonry design code. This conservatism becomes more significant for eccentricity ratios smaller than about 0.4. This finding is in line with the research work conducted by Liu (2002). For plain masonry walls, a constant EI_{eff}/EI_0 value of 0.4 suggested by the code is shown to be very empirical for determining the flexural rigidity values.

The majority of data presented in Figure 5.12 fit in a narrow band formed by two dotted lines also indicated in the figure. This suggests that a general trend of EI_{eff} values exists and it can be reasonably approximated using the lower bound curve.

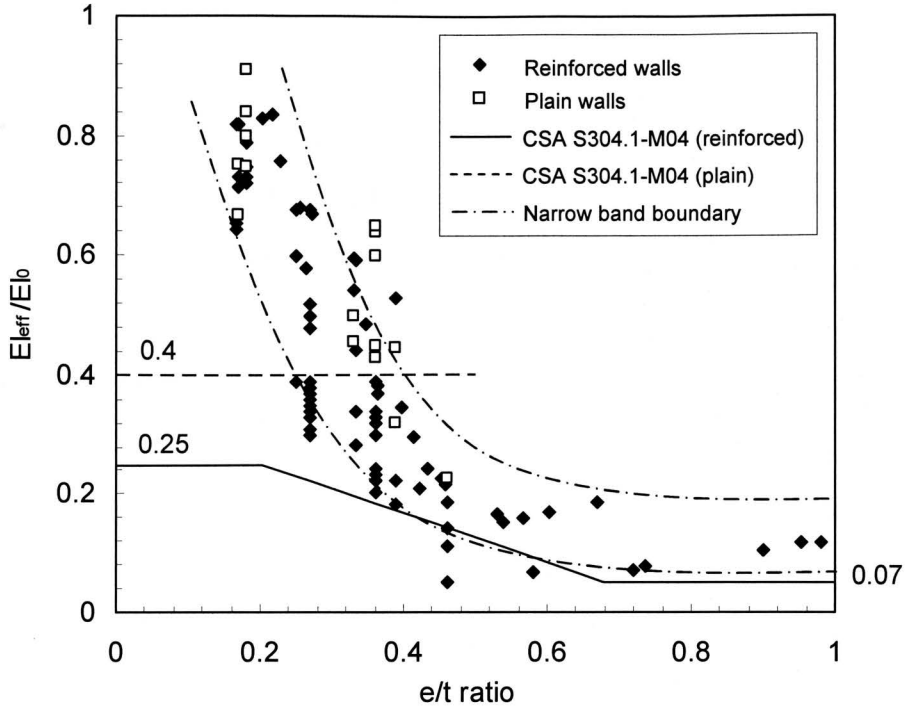

Figure 5.12 EI_{eff}/EI_0 vs. e/t for all available values

In Figure 5.13, EI_{eff}/EI_0 values for masonry walls loaded in symmetrical single curvature with different slenderness ratio, h/t, equal to 8.5, 13.8, 17.1, and 18.0 are plotted against compressive load eccentricity e/t. Although no conclusive comments can be given based only on the comparison presented in the figure, it appears that for a given load eccentricity and end moment ratio, an increase of wall slenderness ratio will result in an increase in flexural rigidity. It is believed that for masonry wall with higher slenderness, the lower ultimate load leads to lower stress levels and less cracking on the cross-section at ultimate, which results in an overall higher flexural rigidity.

The normalized effective flexural rigidity at imminent failure for reinforced masonry walls with three different end moment ratios, e_1/e_2, equal to -1.0, 0.0 and 1.0 are plotted in Figure 5.14 against the end moment eccentricity ratio e/t. Excluding the value for WB-1, the test data included 9 EI_{eff} values of wall specimens obtained from the current

test program and seven values of EI_{eff} obtained by Hatzinikolas et al. (1978) for values of h/t of 17.1 and 18.0. Trend lines are also shown for each series of walls. For masonry walls with similar slenderness ratio, EI_{eff} values for reverse curvature bending walls for eccentricities less than about 0.36 are generally higher. A similar trend can be observed in Figure 5.9. Although more test results are needed to draw a confident conclusion, it is however believed that for masonry walls with constant slenderness ratio, EI_{eff} increases as e_1/e_2 changes from 1.0 to 0.0 and then to -1.0 for a given value of e/t. This is attributed to the reduction in deflection and the extent of related cracking, and the migration of maximum primary moment location toward the end of wall which lead to a reduced secondary moment effect and therefore to a higher effective rigidity. Also noticed in this curve is that in the case of e_1/e_2=-1, the reduction in EI_{eff} as e/t increases is approximately linear.

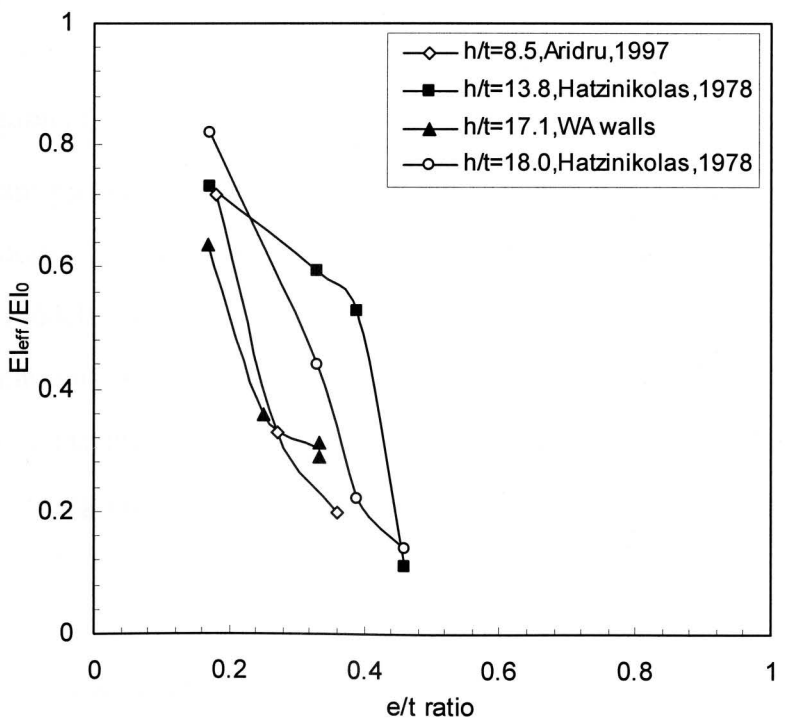

Figure 5.13 EI_{eff}/EI_0 vs. e/t for different slenderness ratios

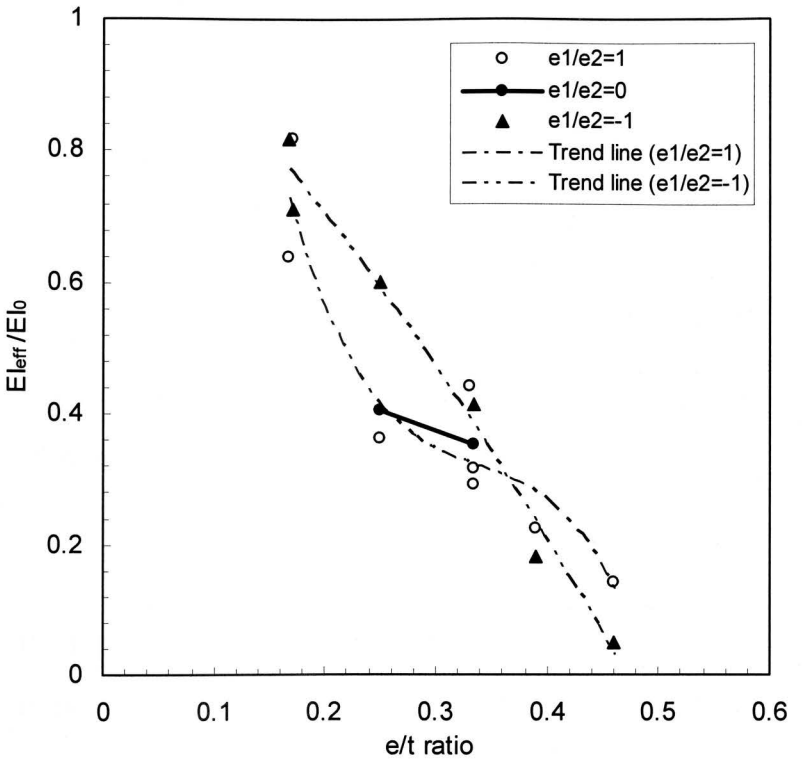

Figure 5.14 EI_{eff}/EI_0 vs. e/t for different end moment conditions

5.3.4.2 Evaluation of various proposed flexural rigidity equations

As an important parameter, the effective flexural rigidity has been the focus of many studies conducted in the past few decades. Many experimental programs and mathematical models have been developed to estimate the effective flexural rigidity of load-bearing masonry walls subjected to combined axial loading and bending. In this section, some of the proposed equations for determining the effective flexural rigidity were evaluated using the available experimental flexural rigidity values presented in the previous section.

Figure 5.15 (a) shows a comparison of the curve determined using Equation (2.11) (MacGregor et al., 1974) with available EI_{eff} values for masonry walls that were reinforced with a single layer of steel rebar and bent in symmetrical single curvature. The

equation specified a lower limit of EI_{eff} equal to $0.10E_mI_0$ for e/t ratios greater than 0.5 and a maximum EI_{eff} of $0.5E_mI_0$ which occurs at e/t=0.0. Hatzinikolas et al. (1978) showed that the moment of inertia and buckling load for plain and reinforced masonry walls loaded in single curvature with eccentricities less than $t/3$ can be approximated by Equation (2.10) which was based on the solution of the governing differential equations. Recognizing the conservatism inherent in the equation when compared with the test results obtained, the equation was modified and expressed as follows for design of eccentrically loaded masonry walls, both plain and reinforced:

$$I = 2I_0\left(\frac{1}{2} - \frac{e}{t}\right) \tag{5.3}$$

In Figure 5.15 (b) Equations (2.10) and (5.3) were plotted along with the experimental values for both plain masonry walls and singly-reinforced walls loaded in single curvature with eccentricities less than one third of the wall thickness.

Equations (2.14), (2.15) and Equations (2.16), (2.17) were proposed by Ojinaga and Turkstra (1980, 1981) to determine the effective moment of inertia of plain masonry wall sections and reinforced masonry walls, respectively. In Figures 5.15 (c) and (d), proposed equations are plotted for masonry walls with end moment eccentricity ratio, e_1/e_2, equals to 1.0, -1.0 and 0.0.

An expression for determining the EI_{eff} values for both reinforced and plain masonry walls was given by Aridru (1997) as Equation (2.18). This expression was established experimentally through a research program with seventy-two plain and reinforced concrete masonry walls with pinned-support conditions tested at various load eccentricities and vertical compressive loading. The comparison between the proposed curves and the collected EI_{eff} values is illustrated in Figure 5.15 (e).

Based on a research program including the experimental results of 36 reinforced concrete masonry walls and numerical analysis of approximately 500 computer model tests, Liu (2002) established an overall lower bound expression for determining the flexural rigidity for reinforced and plain walls under either compressive loading or combined axial and bending. The expression is given as

$$\frac{EI_{eff}}{EI_0} = 0.05 + 0.007\frac{h}{t} + 0.95\exp^{(-\alpha)} \tag{5.4}$$

where, $\alpha = 6\frac{e}{t} + 0.007\frac{h}{t}$

Simplified tri-linear approximation curves for design were also established and are given as Equation (2.19) and Equation (2.21). The two curves are plotted in Figure 5.15 (f), with all collected EI_{eff} values.

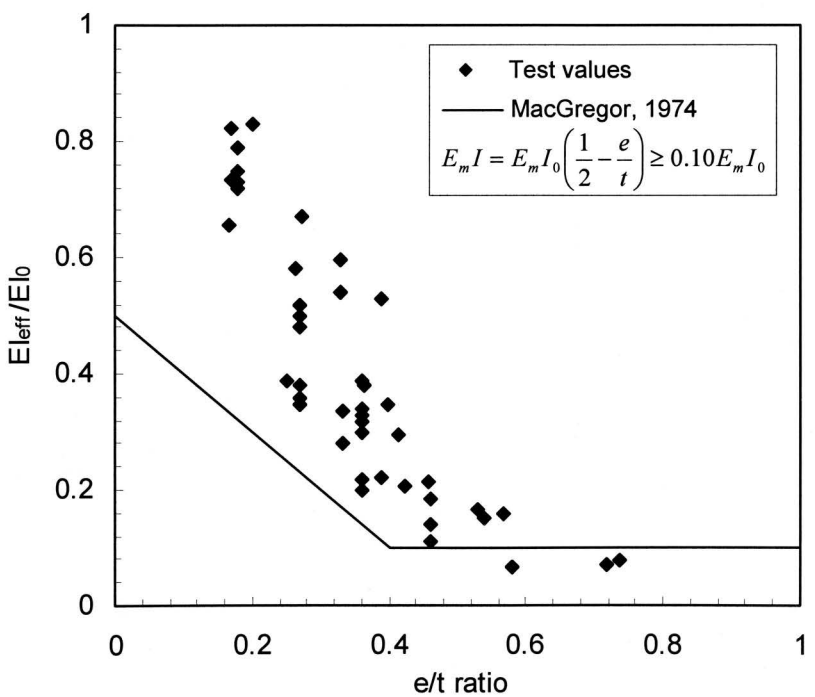

(a) *EI* values for single curvature bending reinforced walls, MacGregor (1974)

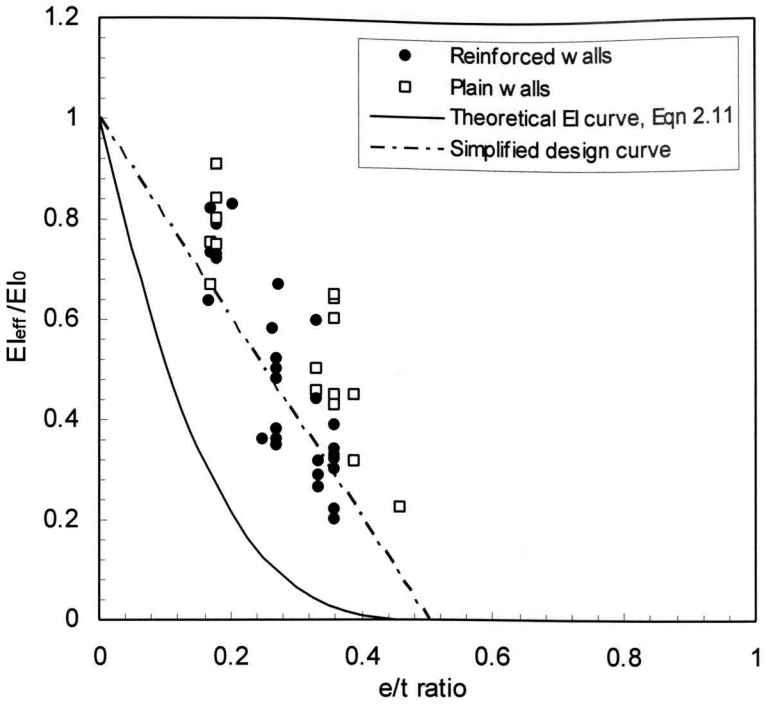

(b) Theoretical *EI* curve and proposed design curve, Hatzinikolas et al. (1978)

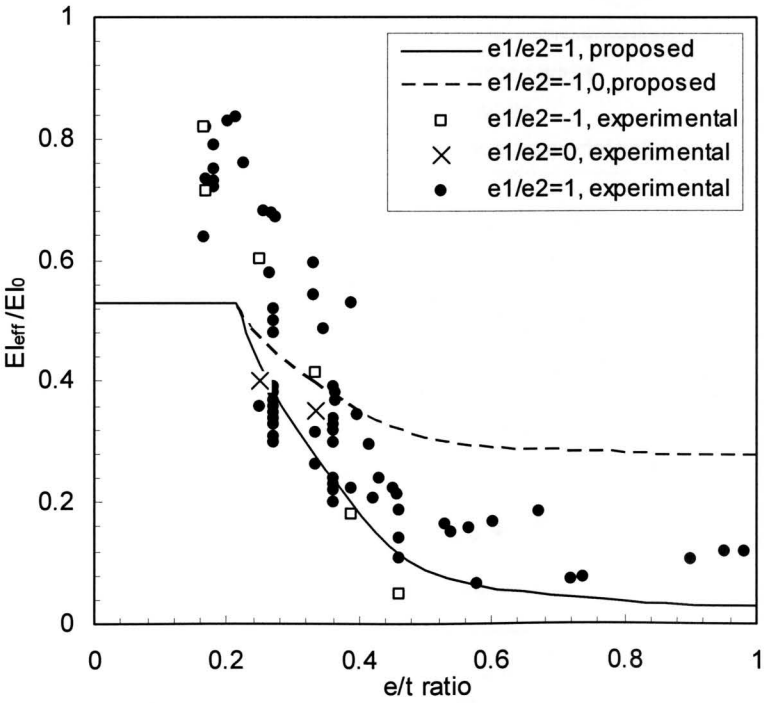

(c) I_{eff} curves for reinforced walls, Ojinaga and Turkstra (1981)

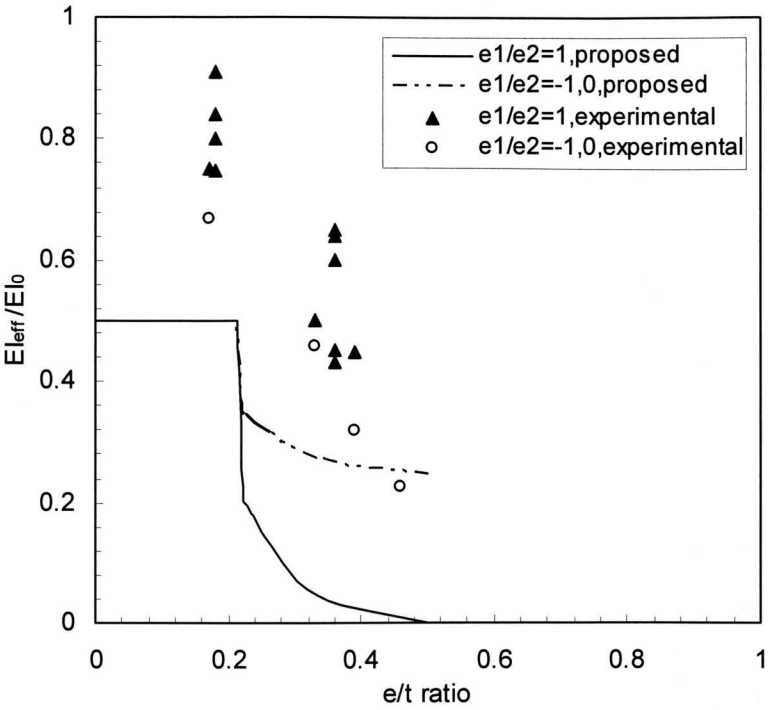

(d) I_{eff} curves for plain walls, Ojinaga and Turkstra (1980)

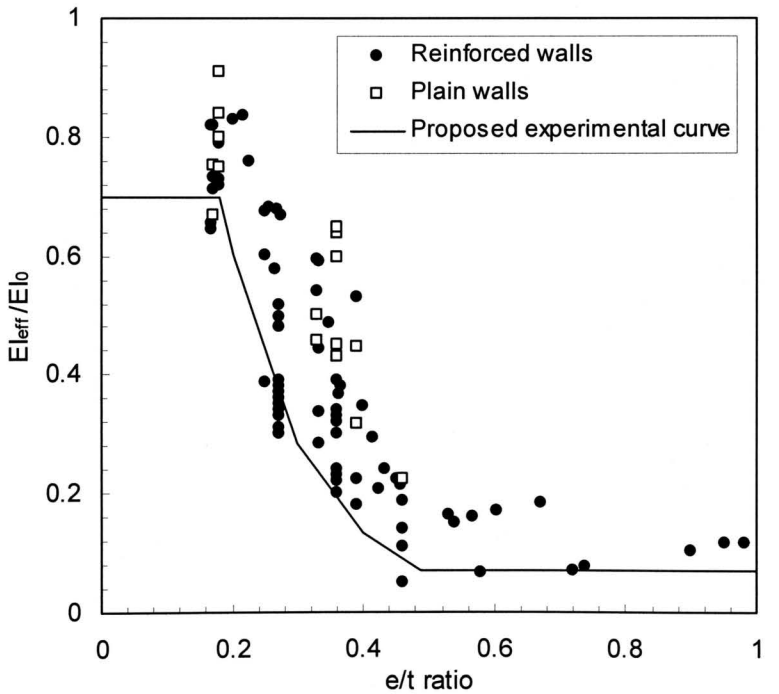

(e) Experimental curve, Aridru (1997)

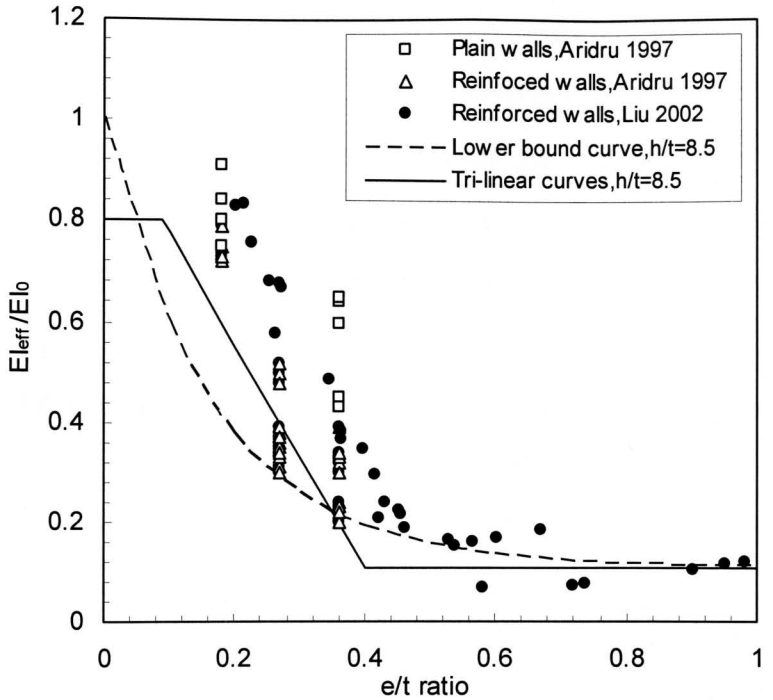

(f) Lower bound curve and tri-linear curves for h/t=17.5, Liu (2002)

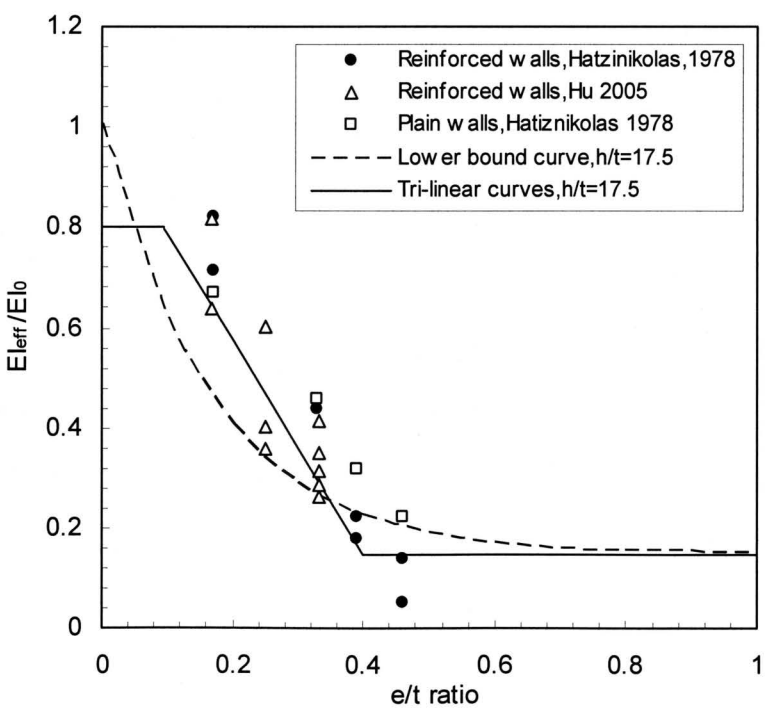

(g) Lower bound curve and tri-linear curves for h/t=8.5, Liu (2002)

Figure 5.15 Comparison between EI_{eff} experimental values and proposed curves

While the simplified design curve expressed as in Equation (5.3) (Hatzinikolas et al., 1978) gives relatively close estimation to the experimental EI_{eff} values, it lacks a rational theoretical derivation. The two curves based on analytical derivation (Equations (2.11) and (2.10)) show the evident conservatism especially for e/t less than 0.4. In addition, since they were derived on the basis of differential equations for symmetrical single curvature bending with pinned-pinned conditions, they may not be appropriate for design of walls subjected to a wide range of load eccentricities and end moment conditions.

The effective moment of inertia equations in Ojinaga and Turkstra (1980, 1981) were proposed for the design of plain masonry and reinforced masonry walls. For predictions of reinforced walls, the expression agrees reasonably well with the lower bound of results for symmetrical single curvature bending walls for eccentricity larger than $0.2t$. For eccentricity less than 0.2t, an upper limit of 0.53 EI_0 was determined form the equation. Ojinaga and Turkstra recognized the higher flexural rigidly for walls tested under asymmetrical single curvature and reverse curvature bending. The two curves plotted for plain masonry flexural rigidity and the flexural rigidity curve for reinforced masonry wall loaded in asymmetrical single curvature and reverse curvature show large disparity with the experimental data.

The experimentally determined EI_{eff} equation given by Aridru (1997) provides a reasonable lower bound estimation for flexural rigidity values for e/t larger than 0.18 as shown in Figure 5.15 (e). This equation indicates that for eccentricity smaller than 0.18 of the wall thickness, the flexural rigidity values are taken as $0.7E_mI_0$, which is arbitrarily selected and lacks experimental and theoretical support.

Figure 5.15 (f) and (g) compared the equations proposed by Liu (2002) and the tested data for slenderness ratios of 18 and 17.1, and 8.5, respectively. While the plotted dashed

curve was determined based on the finite element model tests, a tri-linear simplified curve was also proposed for design as is also shown in the figures. Both curves in Figure 5.15 (f) and (g) correlate well with the test data for a wide range of load eccentricities.

Although all presented equations appear to have reasonably good correlation with the lower bound of the available test data, a further examination of the equations showed that only equations proposed by Liu (2002) have incorporated both eccentricity ratio, *e/t*, and slenderness ratio, *h/t*, as variables in the equation. All other equations include *e/t* as the only variable. Due to the complexity of the problem and limited number of reliable tests, it is recommended that additional research be conducted for a thorough evaluation of the proposed equations. It does appear that a lower bound expression of EI_{eff} may be reasonable for design application at present.

5.4 Concluding Remarks

The capacity of a concrete masonry wall subjected to combined axial loading and out-of-plane bending is influenced mainly by the slenderness ratio, the eccentricities of applied loads, and end moment conditions.

Predicted masonry wall capacities based on rectangular stress-block theory in the design code and moment magnifier method are presented and compared with test results. It is found that the masonry wall cross-sectional strength prediction based on *P-M* interaction diagram were in general conservative in the region of compression-controlled failure but reasonably accurate in the region of tension-controlled failure.

Moment vs. curvature curves for the tested reinforced masonry walls were constructed and the effective flexural rigidities prior to failure were obtained. Test results showed that

EI_{eff} values increase with a decrease of eccentricity ratio. A comparison of the EI_{eff} values for walls with different end moment conditions indicates that for a given load eccentricity, EI_{eff} increases as e_1/e_2 changes from 1.0 to 0.0 and then to -1.0. The effect of end moment conditions is not reflected in the code equations for calculating EI_{eff}.

A total of 101 EI_{eff} values including experimental data obtained from this research and from the available literature were compared with flexural rigidities or recommended by CSA S304.1-04. The validity of several proposed EI_{eff} expressions were evaluated in this chapter. For masonry walls with a given e_1/e_2 ratio and e/t ratio, EI_{eff} increases with an increase in slenderness ratio. A comparison between test data and code values suggests that the code equations underestimate EI_{eff} in the region of e/t less than 0.4, which leads to a conservative design for masonry load-bearing walls failing in compression or combined tension and compression failure.

The evaluation of the various proposed equations showed that, due to the complexity of the problem, most equations use a conservative lower bound curve to estimate the EI_{eff} values. Compromise may be necessary to achieve a simpler expression which is easy for design application.

CHAPTER IV SUMMARY AND CONCLUSIONS

6.1 Summary

This study was undertaken to investigate the behavior of load-bearing masonry walls under combined axial load and out-of-plane bending under various loading conditions. A literature survey revealed that there is a lack of reliable experimental data for walls with high slenderness ratio tested under asymmetrical curvature bending. It was also noted that disparities exist between the available experimental results of wall capacities and values suggested by the current Canadian masonry design code. With the recognition that the moment magnifier method for accounting for secondary effect is a rational approach and easy to use in design, the flexural rigidity, *EI*, as an influential factor in the implementation of the method, was therefore a principal focus of the investigation. The effect on the flexural rigidity and ultimate load of masonry walls of masonry wall slenderness, compressive load eccentricity, and end moment conditions were investigated.

The experimental phase of the study consisted of two parts. The first part included auxiliary tests for determination of masonry component and assemblage properties. Masonry block units, mortar specimens, grout specimens, masonry prisms, and steel reinforcement coupons were tested to determine and maintain the consistency of material properties according to ASTM specifications. In the second part of the experimental program, then large-scale concrete masonry walls were built and tested. Wall specimens were constructed to the dimension of 2390×790×140 mm with the outer two cores grouted and reinforced with 10M rebar. A ccording to the test set-up and boundary conditions of the wall specimens, the slenderness ratio for these walls specimens is 17.1. Three loading conditions including symmetrical single curvature bending, asymmetrical single curvature bending, and reverse curvature bending were considered in the test

program. In addition to a lateral bracing system and transportation assembly, a special set-up for pin support to achieve various required end moment conditions, were designed and fabricated in the program.

Modes of failure as well as results of ultimate load, lateral deflection and moment capacity of wall specimens were presented and discussed. Moment vs. curvature relationships accounted for flexural cracking and nonlinearity of the stress-strain relationship of concrete masonry were obtained based on the experimental results. Strain measurements at the surface of masonry walls were used to determine curvatures at the predicted failure locations, and the values were subsequently used to determine the effective flexural rigidity, EI_{eff}, along with the ultimate moment capacities, which was adjusted to include the secondary moment effect.

The analytical phase of the research program included prediction of masonry wall strength, calculation of effective flexural rigidities prior to failure and evaluation of the various flexural rigidity equations proposed by other researchers and by CSA S304.1-M04 with an emphasis on the effects of important parameters such as slenderness ratios and end moment ratios on flexural rigidity estimation.

6.2 Conclusions

The following conclusions are based on the results of this study:

1. For a given wall slenderness ratio, an increase in the load eccentricity results in a reduction in both the load capacity and the flexural rigidity for the three loading conditions investigated herein. It was found that the reduction is more significant for walls tested under symmetrical single curvature bending than those under asymmetrical single and reverse curvature bending.

2. The reduction of *EI* is a combined result of material non-linearity and reduction of cross-sectional depth due to tensile cracking. The degree of reduction of *EI* is dependent on the interaction between these two effects. The effect of tensile cracking has more pronounced influence on the reduction of *EI* than does the material non-linearity.
3. Eccentric compressive loading was investigated in terms of the variation of e_1/e_2 which reflect the moment gradient over the height of a wall. The load capacity increases as e_1/e_2 changes from positive for single curvature to negative for double curvature. For e_1/e_2=-1, the maximum primary moment occurs at either end of a wall. Thus, the secondary moment due to primary deflection is added to a moment less than the maximum and is less critical than for e_1/e_2=1. Additionally, any physical end constraint that may be present strengthens the end so that the critical section may shift to another location with a lower primary moment but higher moment magnifier tendency. The flexural rigidity, *EI*, increases as e_1/e_2 changes from positive to negative. For a wall bent in reverse curvature, the maximum deflection is restricted in comparison with the same wall bent in single curvature and the failure mode tends towards compression failure. Consequently, the reduction of *EI* is mainly a result of material non-linearity other than steel yielding and masonry tensile cracking. Therefore, a higher *EI* value is obtained than for similar walls bent in single curvature.
4. The strength reduction due to eccentricity required in the flexural theory in CSA S304.1-M04 was found to have been conservative for symmetrical single curvature bending masonry walls tested at eccentricities less than one third of the wall thickness and asymmetrical single and reversed double curvature bending walls.
5. Based on 101 flexural rigidity values, in which nine values were determined in this research program and the remaining ninety-two values were collected from available literature, a comparison between these values and the EI_{eff} values given by CSA

S304.1-M04 revealed that the code equations tend to be conservative for masonry walls with eccentricity ratios smaller than 0.36.

6. The effect of slenderness ratio on EI_{eff} values is inconclusive due to the limited available experimental data. However, it is believed that EI_{eff} tends to increase as the slenderness ratio increases due to the lower degree of inelastic action in a slender wall than in a shorter wall at a given eccentricity.
7. From the EI_{eff}/EI_0 vs. e/t diagram for all the available values, a general trend of variation of these EI values was found to concentrate in a narrow band and a lower bound curve of this narrow band would be an appropriate estimation. A comparison of existing equations and available test data showed that while most proposed equations agree well with the lower bound of the test data, equation by Liu (2002) is the only one which incorporates the slenderness ratio as a variable. More experimental data is needed to further evaluate the accuracy of the equation.
8. It is recommended that some re-assessment of the reduction for slenderness and eccentricities given by CSA S304.1-M04 for the forthcoming limit states code is appropriate. For most cases, it seems that such a re-assessment would lead to increased design capacity for masonry walls.
9. Additional research is required to investigate other possible influential parameters both experimentally and analytically to provide full understanding of the behavior of masonry walls subjected to combined compression load and out-of-plane bending. Future investigation can be conducted to evaluate factors such as wider ranges of wall thickness, slenderness ratios, loading conditions and reinforcement patterns.

REFERENCES

American Society for Testing and Materials, ASTM A 370-02 (2004). Test Methods and Definitions for Mechanical Testing of Steel Products.

American Society for Testing and Materials, ASTM C109/C109M-02 (2004). Standard Test Method for Compressive Strength of Hydraulic Cement Mortars (Using 2-in. or [50mm] Cube Specimens).

American Society for Testing and Materials, ASTM C140-02a (2004). Standard Test Methods for Sampling and Testing Concrete Masonry Units and Related Units.

American Society for Testing and Materials, ASTM C1019-02 (2004). Standard Test Methods for Sampling and Testing Grout.

American Society for Testing and Materials, ASTM C1314-02a (2004). Standard Test Method for Compressive Strength of Masonry Prisms.

American Standards Association Building Code Requirement for Masonry (ASA A41.4-1953) Washington, DC

Aridru, G.G. Effective Flexural Rigidity of Plain and Reinforced Concrete Masonry Walls. Ph.D Thesis. University of New Brunswick. 1997.

CSA Standard CAN3 S304, Masonry Design for Building, Canadian Standard Association, Rexdale, Ontario, 1984

Chapman, J. C., and Slatford, J., The Elastic Buckling of Brittle Columns, Paper No. 6447, Proceedings of the Institution of Civil Engineers, London, Vol. 6, January, 1957, pp. 107-125.

Colville, J., Stability of Hollow Masonry Walls, The Masonry Society, Vol. 11, No. 1, August 1992, pp. 61-74.

Drysdale, R.G., Hamid, A. A., and Baker, A. R., Masonry Structures, Behavior and Design, The Masonry Society, Boulder, Colorado, Second Edition, 1999

Fattal, S. G., Cattaneo, L. E., Structural Performance of Masonry Walls under Compression and Flexure, Building Science Series 73, National Bureau of Standard, Washington, D.C., 1976

Frisch-Fay, R., Stability of Masonry Piers, International Journal of Solid Structures, Vol. 11, 1975, pp. 187-198.

Hatzinikolas, M., Longworth, J., and Warwaruk, J., Concrete Masonry Walls, Structural Engineering Report, Department of Civil Engineering, University of Calgary, Edmonton, Alberta. No.70, September 1978,

LEED for New Construction and Major Renovations (LEED-NC), LEED (Leadership in Energy and Environmental Design) Green Building Rating system, Washington, DC, US, March 2000. Available: http://www.usgbc.org/DisplayPage.aspx?CategoryID=19 [2005, 27 July].

Liu, Y., Beam-column Behavior of Masonry Walls, Ph.D Thesis, University of New Brunswick, Fredericton, Canada, 2002.

MacGregor, J.G., Oelhafen, V. H., and Hage, S. E., A Re-examination of the EI Value for Slender Columns, ACI, SP-50, 1974, pp.1-40

Maksoud, A. A., and Drysdale, R. G., Rational Moment Magnification Factor for Slender Unreinforced Masonry Walls, Proceedings of the 6th North American Masonry Conference, Vol. 1, June 1993, pp.443-454

Masonry Design for Buildings (Limit States Design), CSA S304.1-M94, Canadian Standards Association, Toronto, Ontario, 1994.

Masonry Design for Buildings (Limit States Design), CSA S304.1-M04, Canadian Standards Association, Toronto, Ontario, 2004.

Matlab 7.0.1, The MathWorks, Inc., Cochituate Place, 24 Prime Park Way, Natick, MA 01760, November 2000

National Building Code of Canada 1965 (NBC), Institute for Research in Construction, National Research Council Canada, Ottawa, ON

Ojinaga. J., and Turkstra, C. J., The Design of Plain Masonry Walls, Canadian Journal of Civil Engineering, 7, 1980, pp. 233-242.

Ojinaga. J., and Turkstra, C. J., Design of Reinforced Masonry Walls and Columns for Gravity Loads, Canadian Journal of Civil Engineering, Vol. 9, No. 1, 1981, pp. 84-95.

Romano, F., Ganduscio, S., and Zingone, G., Cracked Nonlinear Masonry Stability under

Vertical and Lateral Loads, Journal of Structural Engineering, ASCE, Vol. 119 No. 1, 1993, pp. 69-87.

Schultz, A. E., and Mueffelman, J. G., Elastic Stability of URM Walls Under Transverse Loading, The Masonry Society Journal, August 2003, pp. 9-19.

The Masonry Standards Joint Committee, Building Code Requirements for Masonry Structures, ACI 530/ASCE5/TMS 402-99, American Concrete Institute, American Society of Civil Engineers, and The Masonry Society, Detroit/New York, 1999.

Yokel, F. Y., Stability and Load Capacity of Members with No Tensile Strength, Journal of the Structural Division, ASCE, Vol. 97, No. ST7, July 1971, pp. 1913-1926.